A decade of marine inorganic carbon chemistry observations in the northern Gulf of Alaska – Insights to an environment in transition

Natalie M. Monacci[1], Jessica N. Cross[2], Wiley Evans[3], Jeremy T. Mathis[4], Hongjie Wang[5]

[1]College of Fisheries and Ocean Sciences, University of Alaska Fairbanks, Fairbanks, AK 99775 USA

[2]Pacific Marine Environmental Laboratory, National Oceanic and Atmospheric Administration, Seattle, WA 98815 USA

[3]Hakai Institute, Campbell River, BC V9W 0B7 Canada

[4]Science, Technology and International Affairs Program, Georgetown University, Washington, DC 20057 USA

[5]Graduate School of Oceanography, University of Rhode Island, Narragansett, RI 02882 USA

Correspondence to: Natalie M. Monacci (nmonacci@alaska.edu)

Abstract. As elsewhere in the global ocean, the Gulf of Alaska is experiencing the rapid onset of ocean acidification (OA) driven by oceanic absorption of anthropogenic emissions of carbon dioxide from the atmosphere. In support of OA research and monitoring, we present here a data product of marine inorganic carbon chemistry parameters measured from seawater samples taken during biannual cruises between 2008 and 2017 in the northern Gulf of Alaska. Samples were collected each May and September over the 10–year period using a conductivity, temperature, depth (CTD) profiler coupled with a Niskin bottle rosette at stations including a long–term hydrographic survey transect known as the Gulf of Alaska (GAK) Line. This dataset includes discrete seawater measurements such as dissolved inorganic carbon and total alkalinity, which allows the calculation of other marine carbon parameters, including carbonate mineral saturation states, carbon dioxide (CO_2), and pH. Cumulative daily Bakun upwelling indices illustrate the pattern of downwelling in the northern Gulf of Alaska, with a period of relaxation spanning between the May and September cruises. The observed time and space variability impart challenges for disentangling the OA signal despite this dataset spanning a decade. However, this data product greatly enhances our understanding of seasonal and interannual variability on the marine inorganic carbon system parameters. The product can also aid in the ground truthing of biogeochemical models, refining estimates of sea–air CO_2 exchange, and determining appropriate CO_2 parameter ranges for experiments targeting potentially vulnerable species. Data are available at https://doi.org/10.25921/x9sg-9b08 (Monacci et al., 2023).

1 Introduction

During the last decade, OA has emerged as one of the most prominent topics in marine research and understanding its potential impacts could be vital for the sustainable management of ecosystem services around the world. The global oceans have become progressively acidified (e.g., Feely et al., 2004; Feely et al., 2009; Jiang et al., 2019) over the last two and half centuries as they have taken up approximately one–fourth of the human output of CO_2 into Earth's atmosphere (e.g., Sabine and Tanhua, 2010; Friedlingstein et al., 2022). At present, the decrease in the average global surface ocean pH averages ~0.1 units, making surface ocean acidity 30% higher than at the start of the Industrial Revolution (Gruber et al., 2023; Jiang et al., 2019). This decline in ocean pH and the sharp rise in seawater carbon dioxide (CO_2) has led to broad reductions in carbonate mineral concentrations in the oceans with diverse, but often detrimental consequences for both pelagic and benthic species (Andrade et al., 2018; Barton et al., 2012; Bechmann et al., 2011; Cooley et al., 2009; Hurst et al., 2012; Hurst et al., 2013; Hurst et al., 2019; Long et al., 2013; Wright–LaGreca et al., 2022).

While acidification is a global phenomenon in the open ocean, there are regional hotspots where natural coastal processes can precondition waters to have lower pH and saturation states for carbonate minerals aragonite and calcite (Ω_A and Ω_C, respectively), creating additive vulnerabilities. Regions where OA is amplified by concurring anthropogenic and natural processes are also interacting with changing temperature, salinity, and gas solubility (Feely et al., 2018). This is particularly true in the high–latitude north Pacific Ocean (e.g., Byrne et al., 2010; Dore et al., 2009) where studies have shown that the region is already experiencing seasonal events where carbonate minerals, such as the biologically important aragonite, can become undersaturated (Evans and Mathis, 2013; Evans et al., 2013; Evans et al., 2014). Models project that under current emission rates large areas of the subarctic Pacific could become undersaturated with respect to aragonite ($\Omega_A < 1$) by as early as mid–century and the entire region will be perennially undersaturated by 2100 (e.g., Gruber et al., 2023; Mathis et al., 2015). The seasonal effects of glacial runoff may also intensify acidification processes because these waters may have naturally low carbonate mineral concentrations depending on how they are discharged into the marine environment (Evans et al., 2014; Reisdorph and Mathis, 2014). Consequently, high–latitude regions provide a real–time laboratory for the evaluation of potential impacts to organisms, and the associated marine resources that they provide (Mathis et al., 2015).

The northern Gulf of Alaska (NGA) is a predominantly downwelling system (Royer and Emery, 1987) with seasonal exceptions. When the onshore surface Ekman transport relaxes in the summer, deep, nutrient–rich, cold water can inundate the continental shelf below the surface layer near shore (Weingartner et al., 2005). The new intermediate water, also enriched in CO_2, causes the saturation horizon for both aragonite and calcite minerals to shoal to within 100 m and 250 m from the surface, respectively (Feely et al., 2004). Along the West Coast of North America, intense wind–driven upwelling can cause the saturation horizon to shoal to the surface over the continental shelf, leaving large, inshore areas exposed to conditions that have been shown to be corrosive to some calcifiers (Bednaršek et al., 2012; Bednaršek et al., 2014; Comeau et al.,

2010). The phenomenon was first observed in the California Current System (Feely et al., 2008), but has also been observed in other high–latitude regions (e.g., Bednaršek et al., 2012; Mathis et al., 2012).

The NGA supports a diverse ecosystem that includes some of the largest commercial fisheries in the world and serves as a pathway for biogeochemical preconditioning of the Bering Sea and Pacific–Arctic region (Cross et al., 2018). The Bering Sea region, like the NGA, supports a highly productive system and these two large marine ecosystems support the largest single–species fishery in the world, walleye pollock (Fissel et al., 2021). On the relatively shallow (<60 m) Bering Sea shelf, there is a natural coupling between surface and bottom waters which is driven by the primary production and respiration signals of large phytoplankton blooms (Mathis et al., 2011a; Mathis et al., 2011b; Mathis et al., 2014). This leads to bottom water conditions where $\Omega_A < 1$ for months at a time, and localized retention of CO_2 can lead to calcite undersaturation ($\Omega_C < 1$; Cross et al., 2013).

When all these factors are considered, it becomes obvious that the NGA is at a critical intersection point for coastally driven OA processes. This issue is of particular importance for the people that rely on marine resources. Alongside these natural vulnerabilities, anthropogenic perturbations may cause ecosystem–level shifts that have the potential to decrease the economic value of commercial fisheries. More than 60% of the catch by weight of United States (U.S.) fisheries are from Alaskan waters (NMFS, 2022) and impacts on commercial and subsistence fishing are equally important topics in marine resources conversations in Alaska (Frisch et al., 2015; Szymkowiak and Steinkruger, 2023). Many communities, particularly those in the NGA region, are vulnerable to risks associated with OA through the loss of culture, jobs, income, and food security (Mathis et al., 2015). Several economically important species have shown negative effects of OA on various developmental stages (e.g., Hurst et al., 2019; Long et al., 2013). Experiments on the economically critical red king crab fishery led to a population dynamics model to predict potential effects on fishery yield (Punt et al., 2014; Punt et al., 2021) and the economic impacts to Alaska (Seung et al., 2015).

To better understand the processes that influence inorganic carbon chemistry and in turn, OA in the NGA, we assembled this decadal time–series data product. Ocean biogeochemical observations, like those we present in this dataset, help researchers determine biogeochemical model performance (e.g., Hauri et al., 2020; Siedlecki et al., 2017), calculate sea–air CO_2 flux (e.g., Evans et al., 2013; Gruber et al., 2023), and set ranges to determine physiological responses to OA on specific species (e.g., Hurst et al., 2013; Long et al., 2013). In turn, these applications can aid in understanding cascading societal impacts of changes in the marine carbonate system, such as determining the vulnerability of a region's marine resources or the effectiveness of marine carbon dioxide removal. We will show how mean water column structure and circulation patterns impact variability in carbon chemistry, discuss some long–term changes in carbon chemistry parameters, and assess the drivers contributing to these patterns of variability as examples of how this data product may be used. In general, we find a pattern of decreasing surface CO_2 during the spring season over time. While our data suggest that this temporal shift is unrelated to temperature patterns, additional research will be required to document a hypothesized change in the timing or

magnitude of the spring bloom that could be leading to these changes. In general, we find that this dataset is good for exploring natural environmental variability in the physical system, and the impacts on carbon parameters.

2 Methods

2.1 Study Area

The GAK Line (Fig. 1) is a long–term oceanographic time–series that has been sampled at least biannually since 1997. The GAK Line is often colloquially referred to as the Seward Line (SL), since the research cruises begin and end from the University of Alaska Fairbanks (UAF) Seward Marine Center in Qutekcak (Seward), Alaska. The SL program began as part of the Northeast Pacific Global Ocean Ecosystem Dynamics (GLOBEC) program, evolved under a funding consortium from 2005–2017, and is currently part of the Northern Gulf of Alaska Long Term Ecological Research (NGA–LTER) project. The northernmost station, GAK1, is at the mouth of Resurrection Bay, with major stations spaced ~20 km apart across the continental shelf to GAK15. In addition to visiting the major stations, most cruises in this dataset began at an inner station, RES2.5, located within Resurrection Bay, and occasionally visited the intermediate (i) stations, spaced every ~10 km from GAK1i to GAK9i.

The GAK Line has two dominant westward circulation features: the Alaska Coastal Current (ACC) and the Alaskan Stream (Fig. 1). The ACC hugs the coast and is driven by freshwater discharge (Childers et al., 2005; Reed, et al., 1987; Royer, 1975) and the Alaska Stream (AS) flows along the continental slope and is driven by the Alaska Gyre (Ladd et al., 2016; Stabeno et al., 2004; Weingartner et al. 2005). The Alaska Gyre controls the circulation in the Gulf of Alaska basin, which responds to the Aleutian Low pressure system and the Pacific Decadal Oscillation. Strengthened seasonal downwelling over the shelf (Royer and Emery, 1987) results from cyclonic wind stress over the Gulf of Alaska basin from the Aleutian Low. Stronger winds and storms associated with the Aleutian Low are typical in autumn, winter, and spring. The resulting downwelling restricts the ACC to a narrow, deep band along the coast (Weingartner et al., 2005) and constructs a shelf break front along the AS (Fig. 2a). Downwelling winds subside in the summer, broadening and shoaling the ACC (Fig. 2b) and allowing a subsurface inflow of cold, nutrient rich Pacific water onto the shelf (Childers et al., 2005; Weingartner et al., 2005). This seasonal relaxation of downwelling presumably allows for longer on–shelf summer residence time of subsurface water that may experience elevated rates of organic matter respiration fueled by high summertime primary productivity.

The Bakun upwelling indices are calculated based on Ekman's theory of mass transport due to wind stress (Bakun, 1973 and 1975; Schwing et al., 1996). Positive values of the Bakun upwelling index are, in general, indicative of upwelling, while negative values imply downwelling. Relative to other upwelling indices broadly available, the Bakun index uses sea level pressure fields from an atmospheric reanalysis to derive estimated near–surface winds. Other indices use winds directly from atmospheric reanalysis that assimilate satellite and *in situ* wind measurements, both of which are limited in the Gulf of

120
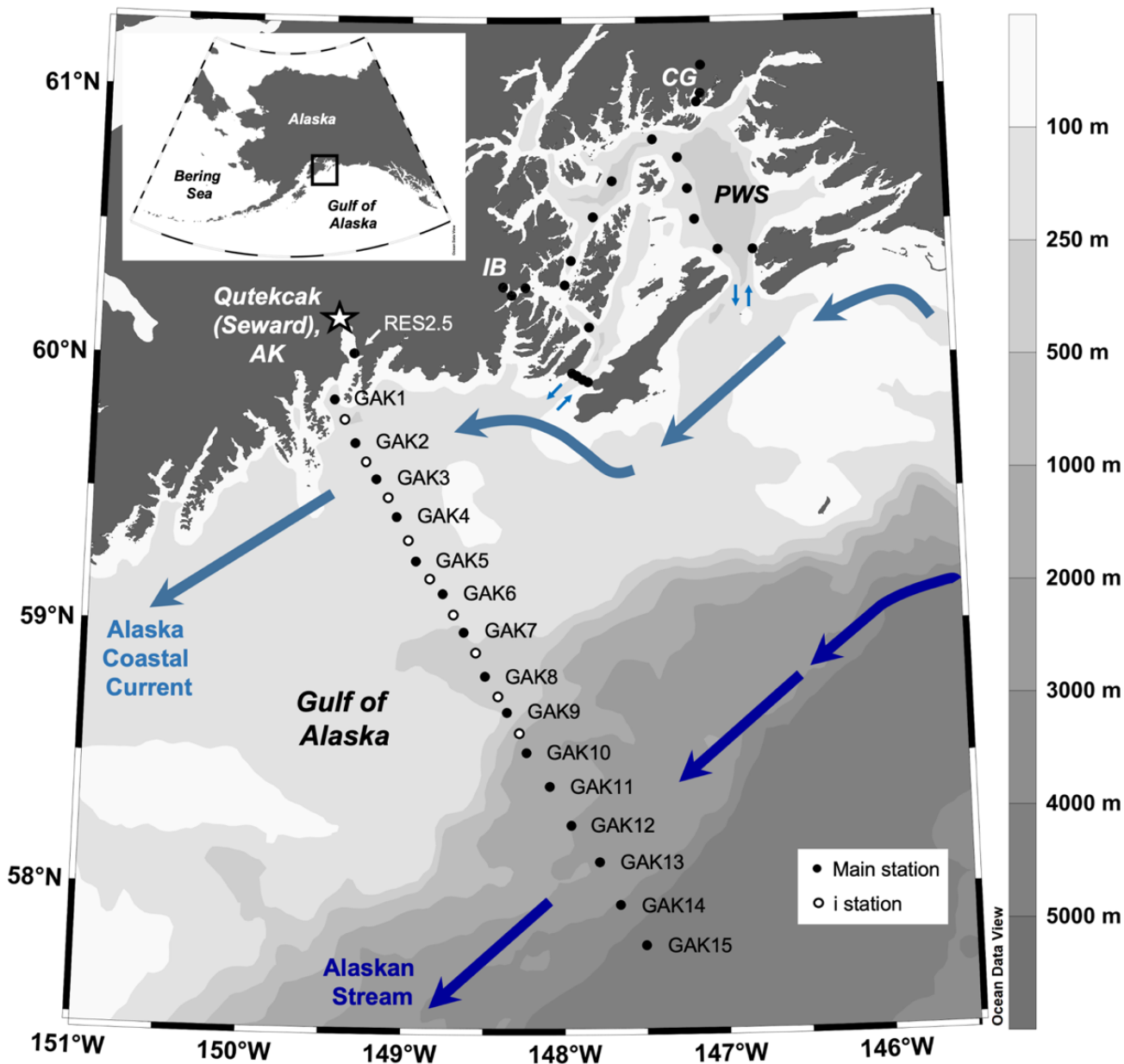
Fig. 1: Map and circulation of study area in the Northern Gulf of Alaska (adapted from Reed et al., 1987). Main Gulf of Alaska (GAK) Line stations 1–15 are mostly sampled each cruise (filled circles), intermediate (i) stations are sampled periodically (open circles). Cruises begin and end in Qutekcak (Seward), AK and occur mostly during the months of May and September. Most cruises also sampled repeat stations in western Prince William Sound (PWS) including the glacially influenced stations in Icy Bay (IB) and near the Columbia Glacier (CG). Nearshore stations are defined as GAK1–2, middle is GAK3–7, and offshore is GAK8–15.

125
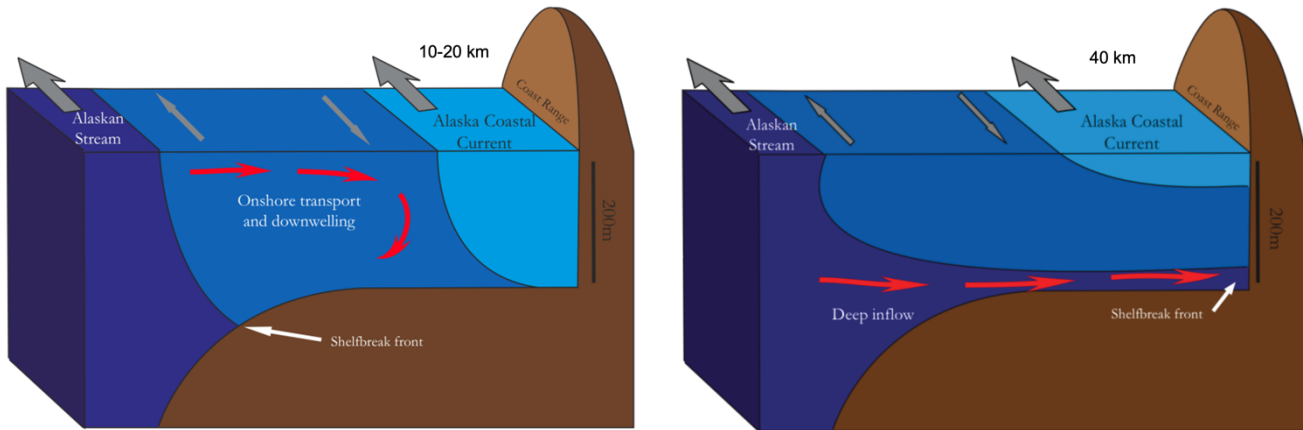
Fig. 2: Northern Gulf of Alaska shelf flow. a) Autumn, winter, and spring shelf flow characterized by onshore transport and downwelling with a relatively narrow (10–20 km) and deep (200 m) Alaska Coastal Current. b) Summer shelf flow characterized by a relaxation of downwelling, allowing the deep inflow of Alaska Stream water under a broader (40 km) and shallower (50 m) Alaska Coastal Current (adapted from Shake 2011).

Alaska basin. However, there are important limitations to the Bakun product: (1) it does not fully account for upwelling driven by wind stress curl (e.g., upwelling associated with alongshore changes in wind), and (2) it does not account for cross–shore geostrophic transport. Other upwelling indices have been developed for the North American west coast (e.g., CUTI and BEUTI, Jacox et al., 2018) which resolve some of these challenges, but which are not available for this geographic region. To provide context for this dataset, here we show annual cumulative downwelling by plotting the cumulative sum of the Bakun Index values over each year (Fig. 3). Bakun upwelling indices for 60° N were obtained from the NOAA Environmental Research Division website: https://oceanview.pfeg.noaa.gov/products/upwelling/dnld. The Cumulative Daily Upwelling Indices (CDUI) for our study area and time show the magnitude and duration of downwelling conditions experienced in the NGA through the year with, importantly, a period of relaxation nominally between May and October.

2.2 Data Collection and Analysis

The biannual cruises in this dataset were typically completed in May and September from 2008 to 2017. Weather, instrumentation, and personnel were the limiting factors to visiting all sampling stations for each cruise. All data presented here were collected using a Seabird 911 Plus conductivity, temperature, and depth (CTD) profiler with a rosette sampler holding twelve, 5 L Niskin bottles. A Seabird 43 dissolved oxygen sensor was included for all cruises after Fall 2011 (TXF11). Temperature (T, ITS–90), Salinity (S, PSS–78), and Oxygen (O_2, Tau and hysteresis corrections applied) bottle data presented here were processed from the upcast profiles using Seabird Scientific Seasoft V2 software.
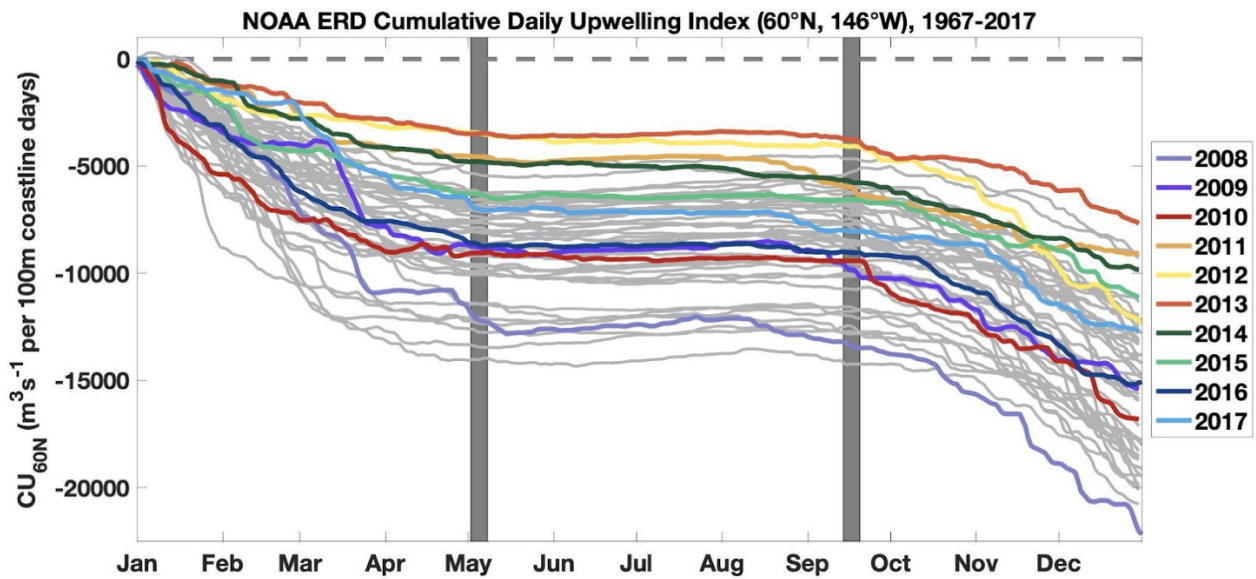
Fig. 3: National Oceanic and Atmospheric Administration (NOAA) Environmental Research Division (ERD) Cumulative Daily Upwelling Index at 60°N, 146°W from 1967 to 2017 (adapted from https://oceanview.pfeg.noaa.gov/products/upwelling/intro). Negative cumulative (CU) values indicate a downwelling system. Study years (2008–2017, color) are highlighted from the full index years (gray). Average cruise dates in May and September are indicated by shaded, vertical bars.

Discrete seawater samples were collected from the Niskin bottles to be analyzed in the laboratory for O_2, dissolved inorganic carbon (DIC), total alkalinity (TA), nutrients (nitrate, nitrite, phosphate, and silicic acid), and stable oxygen isotope ratio ($\delta^{18}O$) of seawater. When collected, discrete O_2 samples were drawn from the Niskin first, following the GO–SHIP Repeat Hydrography Manual (Langdon, 2010) protocol, and analyzed using the Winkler method (Carpenter, 1965; Winkler, 1888) on a Langdon Amperometric titrator at the Ocean Acidification Research Center (OARC) at UAF.

Following the discrete O_2 collection, discrete seawater samples for DIC and TA were drawn from the Niskin into rinsed, borosilicate glass bottles, fixed with saturated mercuric chloride solution, and sealed until analyzed. All DIC and TA samples were analyzed at the OARC at UAF, but methods vary depending on years. DIC samples collected from 2008 to 2013 were analyzed by coulometric titration using a Versatile Instrument for the Determination of Total Alkalinity (VINDTA) 3C paired with a UIC Coulometer. DIC samples collected from 2014–2017 were analyzed using infrared detection with an Automated InfraRed Inorganic Carbon Analyzer (AIRICA) paired with a LiCOR 7000. TA samples were analyzed in an open cell by potentiometric titration using a VINDTA 3C or 3S. All DIC and TA measurements were routinely calibrated using Certified Reference Materials (CRM) from the Dickson Laboratory at the Scripps Institute of Oceanography. Repeat analyses and comparisons across OARC equipment show there was no analytical difference across the various instrumentation used, additional discussion on error is included in Sect. 2.3.

Discrete samples for nutrient analyses were collected and analyzed by various laboratories using similar, though distinct methods. Samples for nutrient analyses collected during cruises in 2008, 2009, 2010, and 2012 were drawn into rinsed, high–density polyethylene (HDPE) vials, frozen at sea, and analyzed at the Whitledge Laboratory at UAF. Here, samples were thawed immediately prior to analyses using colorimetric techniques on a Technicon AutoAnalyzer II and Alpkem model 300 continuous nutrient analyzers (Childers et al., 2005; Whitledge et al., 1981). Samples for nutrient analyses collected during cruises in 2011 and 2013–2015 were syringe–filtered (using 25 mm, cellulose acetate filters with a 0.45 μm pore size) into HDPE vials, frozen at sea, and analyzed at the National Oceanic and Atmospheric Administration (NOAA) Pacific Marine Environmental Laboratory (PMEL). Here, samples were thawed 3–12 hours before analyses according to the methods of Gordon et al. (1993) using a combination of analytical components from Alpkem, Perstorp, and Technicon. Samples for nutrient analyses collected during cruises in 2016 were also filtered using the previously described method but analyzed at OARC at UAF. Here, samples were thawed overnight before being analyzed according to the methods of Gordon et al. (1993) using a SEAL Analytical AA3 continuous flow analyzer. Samples for nutrient analyses collected during cruises in 2017 were filtered and analyzed at the Nutrient Analytical Facility (NAF) at UAF. Here, samples were thawed overnight and brought to room temperature before analyses on a Seal Analytical QuAAtro39 continuous flow analyzer according to methods of Armstrong et al. (1967) and Murphy and Riley (1962). The data we report here are from four macronutrient variables: nitrate, nitrite, phosphate, and silicate (heretofore silicic acid). Silicate data from cruises in 2011 and 2013–2017 had a second analysis performed the following day (first analyses results are not reported) to avoid low values caused by potential polymerization during frozen storage (Burton et al., 1970; Macdonald et al., 1986; Zhang and Ortner, 1998). We believe results from the differing methods used by the various laboratories are mostly comparable, including the filtered vs. non–filtered sampling methods, except for the repeat silicate analysis. Additional discussion of the variability in these methods is included below in Sect. 2.3 and 2.4.

Stable oxygen isotope ($\delta^{18}O$) samples were collected in borosilicate glass vials with no headspace, sealed with parafilm, and submitted to the Stable Isotope Laboratory (SIL) at Oregon State University (OSU). All $\delta^{18}O$ values are reported relative to Vienna Standard Mean Ocean Water (VSMOW).

2.3 Data organization and manipulation

This data product merges the GAK Line data from 20 cruise–level archived datasets (Table 1; Monacci et al., 2020a–j) and is organized using best practice data standards including column header abbreviation standards from Jiang et al. (2022; Table 2). A sample identifier (sample ID) is generated to create a value unique to each EXPOCODE to easily incorporate data into data products such as the Coastal Ocean Data Analysis Product in North America (CODAP–NA; Jiang et al., 2021). The sample ID uses the formula outlined by Jiang et al., 2021 and is calculated following Eq. (1):

$$Sample\ ID = Station\ ID \times 10{,}000 + Cast\ number \times 100 + Rosette\ position \qquad (1)$$

EXPOCODE	Cruise	Ship	Start Date	End Date	DOI	CRM batch	TA	DIC	Nutrients	O_2	$\delta^{18}O$	i
33A020080502	TXS08	M/V Tiĝlax̂	05/02/08	05/06/08	https://doi.org/10.25921/44kh-zb66	82			UAF-WL*			
33A020080913	TXF08	M/V Tiĝlax̂	09/13/08	09/16/08	https://doi.org/10.25921/44kh-zb66	82			UAF-WL*			
33A020090503	TXS09	M/V Tiĝlax̂	05/03/09	05/08/09	https://doi.org/10.25921/n43y-9r47	96			UAF-WL*			x
33A020090914	TXF09	M/V Tiĝlax̂	09/14/09	09/19/09	https://doi.org/10.25921/n43y-9r47	96			UAF-WL*			x
32QO20100503	N2S10	R/V Norseman II	05/03/10	05/07/10	https://doi.org/10.25921/avxr-m571	99			UAF-WL*			
33A020100914	TXF10	M/V Tiĝlax̂	09/14/10	09/18/10	https://doi.org/10.25921/avxr-m571	99			UAF-WL*			x
33A020110506	TXS11	M/V Tiĝlax̂	05/06/11	05/09/11	https://doi.org/10.25921/07yn-b044	108			PMEL			
33A020110915	TXF11	M/V Tiĝlax̂	09/15/11	09/19/11	https://doi.org/10.25921/07yn-b044	112			PMEL	x	x	x
33A020120503	TXS12	M/V Tiĝlax̂	05/03/12	05/09/12	https://doi.org/10.25921/mttc-gc63	114, 119	6.85	6.32	UAF-WL*	x	x	x
33A020120913	TXF12	M/V Tiĝlax̂	09/13/12	09/18/12	https://doi.org/10.25921/mttc-gc63	120	4.3	3.9	UAF-WL*	x		x
33A020130427	TXS13	M/V Tiĝlax̂	04/27/13	05/08/13	https://doi.org/10.25921/n5dy-h455	121, 126	3.15	5.18	PMEL	x	x	x
33A020130914	TXF13	M/V Tiĝlax̂	09/14/13	09/26/13	https://doi.org/10.25921/n5dy-h455	128, 129	2.68	2.15	PMEL	x	x	
33A020140503	TXS14	M/V Tiĝlax̂	05/03/14	05/08/14	https://doi.org/10.25921/ke3w-xp11	134, 135	4.21	2.98	PMEL	x	x	
33A020140913	TXF14	M/V Tiĝlax̂	09/13/14	09/19/14	https://doi.org/10.25921/ke3w-xp11	140, 141	12.72	11.56	PMEL	x		
33A020150505	TXS15	M/V Tiĝlax̂	05/05/15	05/11/15	https://doi.org/10.25921/r7kp-0j46	144	8.56	7.51	PMEL	x		
33A020150914	TXF15	M/V Tiĝlax̂	09/14/15	09/20/15	https://doi.org/10.25921/r7kp-0j46	144, 146			PMEL	x		
33A020160430	TXS16	M/V Island C†	04/30/16	05/27/16†	https://doi.org/10.25921/ed32-3h29	146, 148	2.57	4.59	UAF-OARC	x		
33A020160915	TXF16	M/V Tiĝlax̂	09/15/16	09/20/16	https://doi.org/10.25921/ed32-3h29	148			UAF-OARC	x		
33A020170501	TXS17	M/V Tiĝlax̂	05/01/17	05/08/17	https://doi.org/10.25921/rvm1-vj65	157, 165, 169	5.81	7.22	UAF-NAF	x		
33A020170916	TXF17	M/V Tiĝlax̂	09/16/17	09/22/17	https://doi.org/10.25921/rvm1-vj65	164, 165, 170	4.59	4.02	UAF-NAF	x		

205 | Table 1: List of cruises used to produce this data product. EXPOCODE: Expedition code consists of the four–digit International Council for the Exploration of the Sea (ICES) platform code and the date of departure from port (UTC) in YYYYMMDD. Cruise: The project Cruise name, including the letters of the ship (TX = R/V *Tiĝlax̂*), the northern hemisphere season (S = Spring, F = Fall), and the year in format YY (2008 = 08). Ship: Vessel name used for field work, where † indicates the R/V *Tiĝlax̂* experienced engine problems and the M/V *Island C* was chartered in late May to occupy stations GAK2–15, though no DIC/TA samples were collected. Start Date and End Date: UTC in DD/MM/YY. DOI: Digital Object Identifier (Monacci et al., 2020a-j). CRM Batch: Batch numbers of the Certified

210 | Reference Materials. TA and DIC: Mean uncertainty of triplicate discrete samples in μmol kg^{-1}. Nutrients: Laboratory where analysis of discrete nutrient samples were analyzed (UAF-WL = University of Alaska Fairbanks Whitledge Lab, PMEL = Pacific Marine Environmental Laboratory, UAF-OARC = UAF Ocean Acidification Research Center, UAF-NAF = UAF Nutrient Analytical Lab), where * indicates all nutrient values are QF = 3 and are not included in this merged data product. O_2, $\delta^{18}O$, i: Dissolved oxygen, stable oxygen isotope ratio, and GAK

215 | Line i stations, where x indicates data was collected. All files include data with variables CTDTEMP, CTDSAL, DIC†, TA†, Silicate, Phosphate, Nitrate, and Nitrite, except when indicated otherwise. Columns O_2 and $\delta^{18}O$ marked with x indicate that variables CTDOXY, OXYGEN, and DEL18O are included. Column GAK i marked with x indicate the GAK intermediate (i) stations were visited.

Abbreviation	Variable description	Unit
CTDPRS	Pressure recorded from sensors on CTD.	dbar
CTDTMP_ITS90	Temperature on the International Temperature Scale of 1990 (ITS-90) from the sensors on CTD.	°C
CTDSAL_PSS78	Salinity on the Practical Salinity Scale 1978 (PSS-78) calculated from the conductivity sensor on CTD.	
CTDOXY	Dissolved oxygen measured from sensors on CTD.	μmol kg^{-1}
OXYGEN	Dissolved oxygen measured from discrete samples.	μmol kg^{-1}
TA	Total Alkalinity measured from discrete samples.	μmol kg^{-1}
DIC	Dissolved Inorganic Carbon measured from discrete samples.	μmol kg^{-1}
Silicate	Silicate measured from discrete samples.	μmol kg^{-1}
Nitrate	Nitrate measured from discrete samples.	μmol kg^{-1}
Nitrite	Nitrite measured from discrete samples.	μmol kg^{-1}
Phosphate	Phosphate measured from discrete samples.	μmol kg^{-1}
DELO18	Stable oxygen isotope ratio measured from discrete samples.	‰

Table 2: Parameters included in this data product (adapted from Jiang et al., 2021).

220 | When samples are collected at i stations, a half value is used. For example, at station GAK1i, the sample ID is 1.5, giving the sample collected at GAK1i, cast 3, Rosette position of 11 a Sample ID of 15311. Stations visited off the GAK Line,

including repeat stations visited in most years within Prince William Sound (PWS, Fig. 1) and stations of opportunity, are not included in this data product. See Sect. 4 for additional information on stations and data collected outside the GAK Line.

Quality control (QC) steps on the cruise–level files follow previous studies (e.g., Jiang et al., 2021; Tanhua et al., 2010).
225 First, the 'zero step' QC is performed on individual measurements from instruments during collection. Next, the primary QC level used property–property plots to eliminate any outliers. Finally, we added an additional step to identify questionable data based on expected values using the regression according to Evans et al. (2013). Here we applied a multiple linear regression (MLR) based on an O_2–based algorithm to predict DIC. Then, we compared the derived DIC from our predictions to measured DIC to isolate measurements where the difference between measured and predicted values exceeded 4 times the
230 root mean square error (RMSE) of the algorithm. The final QC step applied in this dataset is not comparable to the secondary level QC flags for global products such as the Global Ocean Data and Analysis Product (GLODAP, Lauvset et al., 2022). Both GLODAP and CODAP–NA use an additional QC process to identify biases in the data (Olsen et al., 2016 and 2017). The data in this product have not been converted or corrected in any way for potential systematic biases.

Quality flags (QF) were applied to the cruise–level files according to best practices outlined in Jiang et al. (2022) and
235 summarized in Table 3. This data product and corresponding figures in this publication only include GAK Line data when the measured carbonate parameters (TA and DIC) had a QF = 2 ("acceptable"). No data identified as QF = 3 ("questionable") or QF = 4 ("known bad") are included in the merged data product. Due to inconsistencies in nutrient sample collection and analysis methods on samples from cruises in 2008, 2009, 2010, and 2012, these data were assigned a QF = 3 in the original cruise–level files and are also excluded from this data product (indicated by the * in the nutrients column in
240 Table 1). This data product (Monacci et al., 2023) used "–999" and QF = 9 ("not reported") when the cruise–level data was assigned a QF other than 2. The individual cruise datasets include all data (Monacci et al., 2020a–j).

Flag	Meaning
2	Acceptable
3	Questionable
4	Known Bad
6	Average value
9	Missing value

Table 3: Summary of standard primary level quality control flags (Jiang et al., 2022) in this data product.

2.3 Calculations and Error

Using the analytical accuracy and precision of the Marine Analytics and Data (Marianda) built instruments, VINDTA and
245 AIRICA, the uncertainty was calculated in quadrature using Eq. (2):

$$Uncertainty = \sqrt{accuracy^2 + precision^2} \tag{2}$$

The mean handling error for TA and DIC are 5.54 ± 3.15 μmol kg^{-1} and 5.54 ± 2.74 μmol kg^{-1}, respectively, which is larger than the mean analytical uncertainty. Mean handling error, calculated from the triplicate discrete samples collected from the same Niskin bottle on most cruises (Table 1) are assumed to be representative of both sampling and storage uncertainties. Analytical precision and accuracy and the handling error we report here are averaged for all 20 cruise–level datasets. The mean analytical uncertainty for our measured variables, TA and DIC, are 2.82 μmol kg^{-1} and 3.10 μmol kg^{-1}, respectively (Table 4).

Measured	Mean uncertainty
TA	2.82 μmol kg^{-1}
DIC	3.10 μmol kg^{-1}

Calculated	Mean uncertainty
fCO$_2$	4.0 %
Ω_A	5.5 %

Table 4: Mean uncertainties of parameters calculated in CO2SYS. Input parameters are *in situ* T, S, and pressure and measured TA, DIC, phosphate and silicate. Mean analytical uncertainties for the measured parameters DIC and TA are in quadrature, combining the accuracy and precision of the instruments.

Due to a low number of samples collected below 1500 m water depth, we were not able to perform a crossover analysis on deep water property variability. Therefore, the most recently developed tool (Jiang et al., 2021) for inter–cruise comparisons and internal consistency was not used, and we do not have an inter–cruise error estimate as produced on other multi–cruise projects (e.g., Gouretski and Jancke, 2001; Johnson et al., 2001; Olsen et al., 2016). The internal consistency of the dataset is challenged in multiple ways, including the various methods used to sample and analyze nutrient measurements, as discussed above. However, it also routinely challenged the capacity of samplers to collect data relevant for inter–cruise comparisons. Deep water sampling requires wire time not just for the CTD cast itself, but also weather windows and conditions that allow for sampling at the deepest station (GAK15). Accordingly, deep water data in this dataset that could have been used for the calculation of internal consistency was only available in the early part of the dataset (before 2014). Furthermore, the low sample number (n; Table 5) of these samples also challenges the creation of a statistical mean against which a potential bias of each cruise could be measured. Accordingly, no bias in individual cruises was identified, and no correction for internal consistency was applied to any single mission in this dataset. Despite these high errors in deep water sampling, note that there is sufficient surface water data to explore climatological changes with statistical significance elsewhere in this dataset.

Season	Sample depth (m)	TA (μmol kg^{-1})	DIC (μmol kg^{-1})	n
All	< 950	2378 ± 21	2357 ± 25	52
	999-1022	2375 ± 23	2355 ± 27	34
	>1400	2390 ± 12	2366 ± 16	13
Spring	< 950 m	2387 ± 29	2367 ± 22	18
	999-1022	2385 ± 34	2367 ± 25	12

	>1400	2392 ± 10	2368 ± 13	6
Autumn	< 950	2375 ± 17	2352 ± 27	36
	999-1022	2370 ± 11	2349 ± 26	22
	>1400	2389 ± 14	2364 ± 19	7

Table 5. Deep water data used for the demonstration of internal consistency, including the average and standard deviation of DIC (μmol kg^{-1}) and TA (μmol kg^{-1}) data below 950 m, between 999 and 1022 m, and deeper than 1400 m across the entire dataset, in spring, and in autumn. The number of samples used to derive these statistics is also shown.

We used a MATLAB version of CO2SYS (van Heuven et al., 2011) to calculate the fugacity of carbon dioxide (fCO$_2$), pH on Total Scale (pH$_T$), and saturation state for aragonite (Ω_A) when the measured input variables (T, S, DIC, TA, phosphate, and silicate) had a QF = 2. In years where no nutrient data met the QF = 2 criteria (e.g., 2008, 2009, 2010, 2012), we included a seasonal average nutrient value for that location and depth in the calculation. The nutrient alkalinity increases the fCO$_2$ and reduces the carbonate ion (CO$_3^{2-}$) value when the DIC–TA input pair is used (Orr et al., 2015), therefore, the averaged nutrient values are a better estimation than not including phosphate and silicate values. We applied the K$_1$ and K$_2$ stoichiometric constants from Millero et al. (2006), the K$_{SO4}$ dissociation constant from Dickson (1990), and the K$_B$ constant from Uppström (1974). New software packages have the capacity to compute propagated uncertainties (Dillon et al., 2020; Orr et al., 2018; Sharp and Byrne, 2021) for the calculated parameters. Using the Orr et al. (2018) application with average input values from this data product and the reference uncertainties results in percent relative combined standard uncertainty of nearly 4.0 % for fCO$_2$ and 5.5 % for Ω_A (Table 4).

2.4 Determining controls on surface fCO$_2$

We follow the approach by Wang et al. (2022), a modified method first developed by Takahashi et al. (2002), to calculate the interannual fCO$_2$ variability drivers, as well as the influence of sea surface temperature (T) and all other non–thermal processes (nT) on the fCO$_2$ anomaly using Eq. (3) and Eq. (4):

$$T(\Delta fCO_2) = fCO_2 - nfCO_2 \tag{3}$$

$$nT(\Delta fCO_2) = nfCO_2 - fCO_{2\,mean} \tag{4}$$

Like Wang et al. (2022), the T and nT in this study are different from the thermal and non–thermal fCO$_2$ components calculated in Takahashi et al. (2002) due to the unavailability of annual mean fCO$_2$ in high latitudes. Note that Eq. (4) is different from Wang et al. (2022) as we are calculating seasonal means of fCO$_2$, not ocean-atmosphere flux (F). Therefore, the quantity fCO$_{2\,mean}$ represents the climatological spring or autumn means of fCO$_2$ and nfCO$_2$ is the temperature–normalized fCO$_2$ relative to the climatological mean spring or autumn temperature using Eq. (5):

$$nfCO_2 = fCO_2 \times exp\ (0.0423(T_{mean} - T_{obs}))$$ (5)

Equation (5) is from Takahashi et al. (2002), where T_{obs} is the *in–situ* temperature, and T_{mean} (Fig. 4) is the climatological spring or autumn mean value. Wang et al. (2022) explains that Eq. (3) is a measure of the temperature effect, relative to the climatological seasonal mean temperature and Eq. (4) represents the impact of processes (e.g., biological CO_2 consumption or respiration, ocean-atmosphere CO_2 flux, and changes in carbonate ion concentrations) unrelated to temperature (e.g., Bates et al., 2013, Cross et al., 2013). Lastly, we calculate the fCO_2 anomaly using Eq. (6):

$$fCO_{2\,anomaly} = fCO_{2\,ocean} - fCO_{2\,mean} = T(\Delta fCO_2) + nT(\Delta fCO_2)$$ (6)
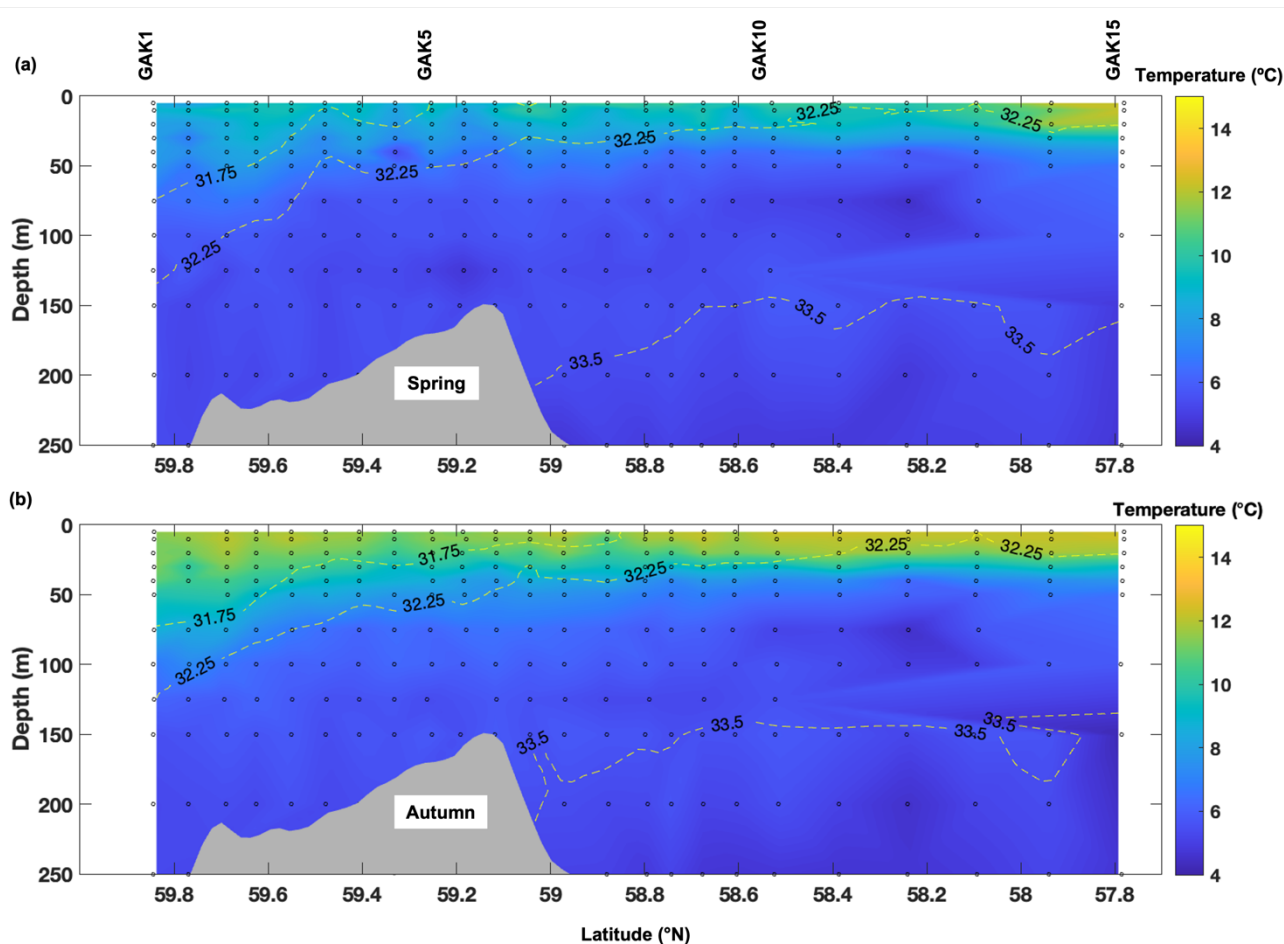
Fig. 4: a) The climatological average seawater temperature in the upper 250 m of the GAK Line transect in a) spring (May) and b) autumn (September) during all study years (2008–2017), plotted with salinity contours.

3 Dataset Demonstration

In this section, we offer some examples of the value and potential usages of this dataset for evaluating carbonate chemistry patterns and discuss how additional data collections may improve the quality, usability, and accessibility of the dataset. At present, we estimate that the value of this time series will be primarily for the exploration of climatological patterns in carbonate chemistry parameters. Below, we offer a climatological exploration of fCO_2 as an example. In general, we find that this dataset is of sufficient length and quality to determine some climatological trends in fCO_2, as well as to assess some of the potential physical drivers of this variability. However, physical parameters, such as temperature, do not sufficiently describe these emerging trends. Additional datasets and analysis will be necessary to identify the mechanisms that underpin these changes. Overall, this dataset is good for exploring climatological mean states, some geochemical trends and variability, and the physicochemical contributions to this variability, but not for assessing potential biological contributions to carbon system variability, the physicochemical contributions to this variability, but not for assessing potential biological contributions to carbon system variability.

3.1 Seasonality of fCO_2

The average spring (a) and autumn (b) fCO_2 along the GAK Line are shown in Fig. 5. In general, seasonality was more evident in the intermediate depths (50–200 m), likely due to the known seasonal oscillation in downwelling strength. For example, 50% of autumn fCO_2 values fell in the 683–980 µatm range, which was slightly higher than the values from spring (600–967 µatm). By contrast, the average surface (upper 50 m) fCO_2 did not vary seasonally. The average surface fCO_2 in spring ranged from 247 µatm to 450 µatm, with 50% of data ranging from 309 to 363 µatm, lower than the atmospheric level. The average surface fCO_2 in autumn was almost identical to spring, but with a few extreme outliers (460–528 µatm) because of episodic mixing events that brought higher fCO_2 from the deep layer to the surface layer. The median fCO_2 in the average surface layer in spring and autumn were 329 µatm and 336 µatm, respectively. This average surface fCO_2 value is lower than atmospheric fCO_2, again indicating this region is a year–round CO_2 sink, as previously documented (Evans and Mathis, 2013).

3.2 Climatology of surface fCO_2

The climatological average fCO_2 in the surface (upper 50 m) was lower than the atmospheric fCO_2 value (Fig. 6), with episodic high fCO_2 events (>450 µatm) in both seasons. Interestingly, there were more episodic high fCO_2 values before 2014 in both seasons. Based on a temperature normalization analysis, temperature seems not to be the primary driver of either the long–term decline in average surface fCO_2 or the frequency and magnitude of the episodic high fCO_2 events. The $T(\Delta fCO_2)$ represents the impact of temperature anomalies on surface fCO_2. As temperature anomalies increase, fCO_2 and
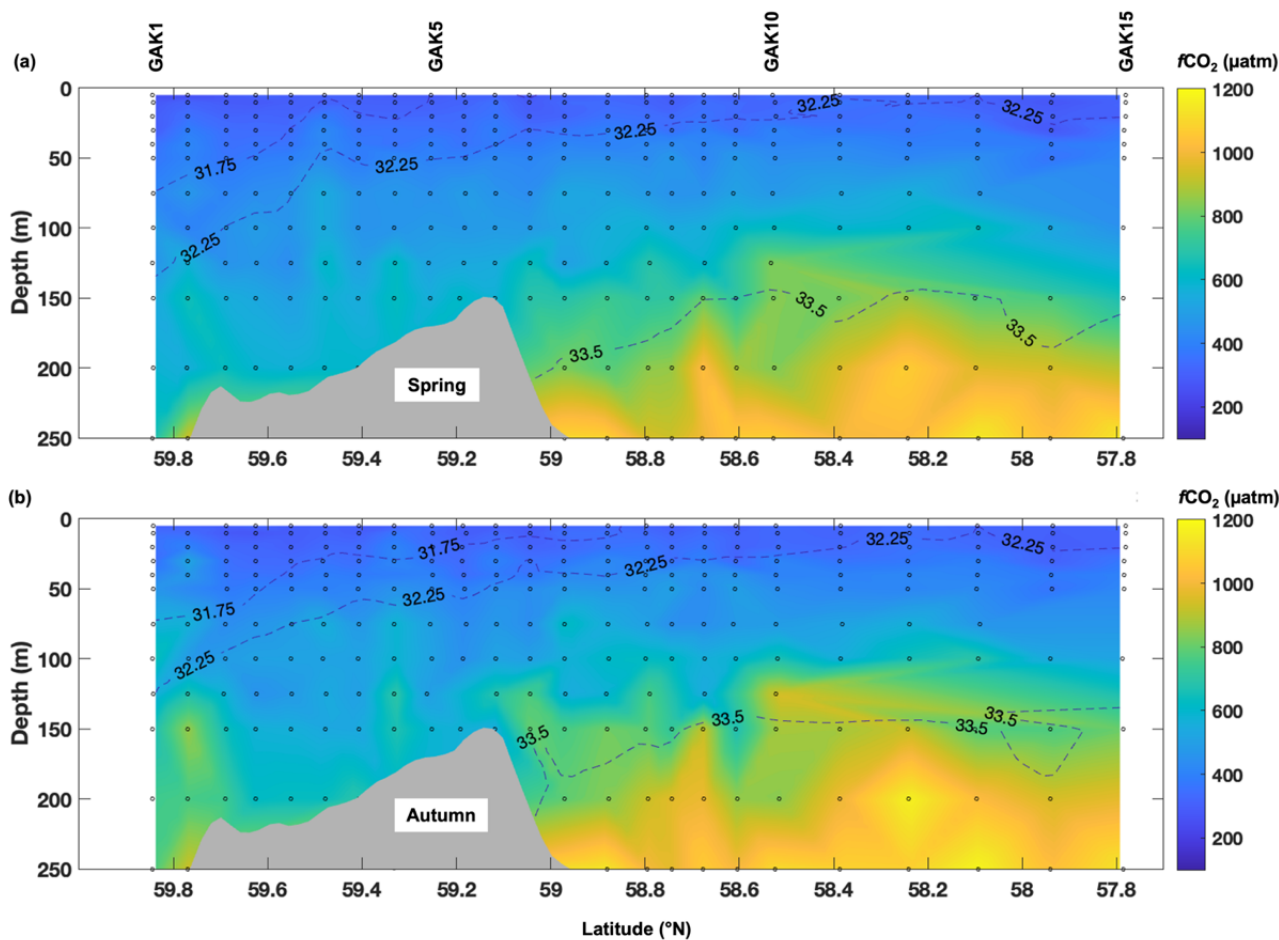
Fig. 5: a) The average fugacity of carbon dioxide (fCO_2) in the upper 250 m of the GAK Line transect in a) spring (May) and b) autumn (September) during all study years (2008–2017), plotted with salinity contours.

T(ΔfCO_2) increase first due to a decrease in CO_2 dissolution. This is further compounded by shifts in equilibrium that favor reactants, specifically, CO_2 and H_2O, over their product forms (H_2CO_3, HCO_3^-, and CO_3^{2-}). Consequently, more CO_2 remains in its initial, unreacted state. However, there were no clear temporal changes from T(ΔfCO_2) between before 2014 and after 2014, anomalies were less than 50 µatm, which cannot explain the >200 µatm episodic changes. Therefore, our analyses suggest that other nonthermal processes, such as anomalies in productivity/respiration, may well lead to interannual variations in surface fCO_2. Anomalies in the patterns of primary productivity and respiration may, at least to a first order, be related to patterns in regional wind forcing, and we note that 2011–2013 displayed some of the weakest CDUI values over the start of each year in this dataset (Fig. 2). Weaker CDUI values over the first half of the year would imply reduced winter downwelling and storm activity, which acts to replenish surface nutrients. A reduction in stormy conditions would pre-
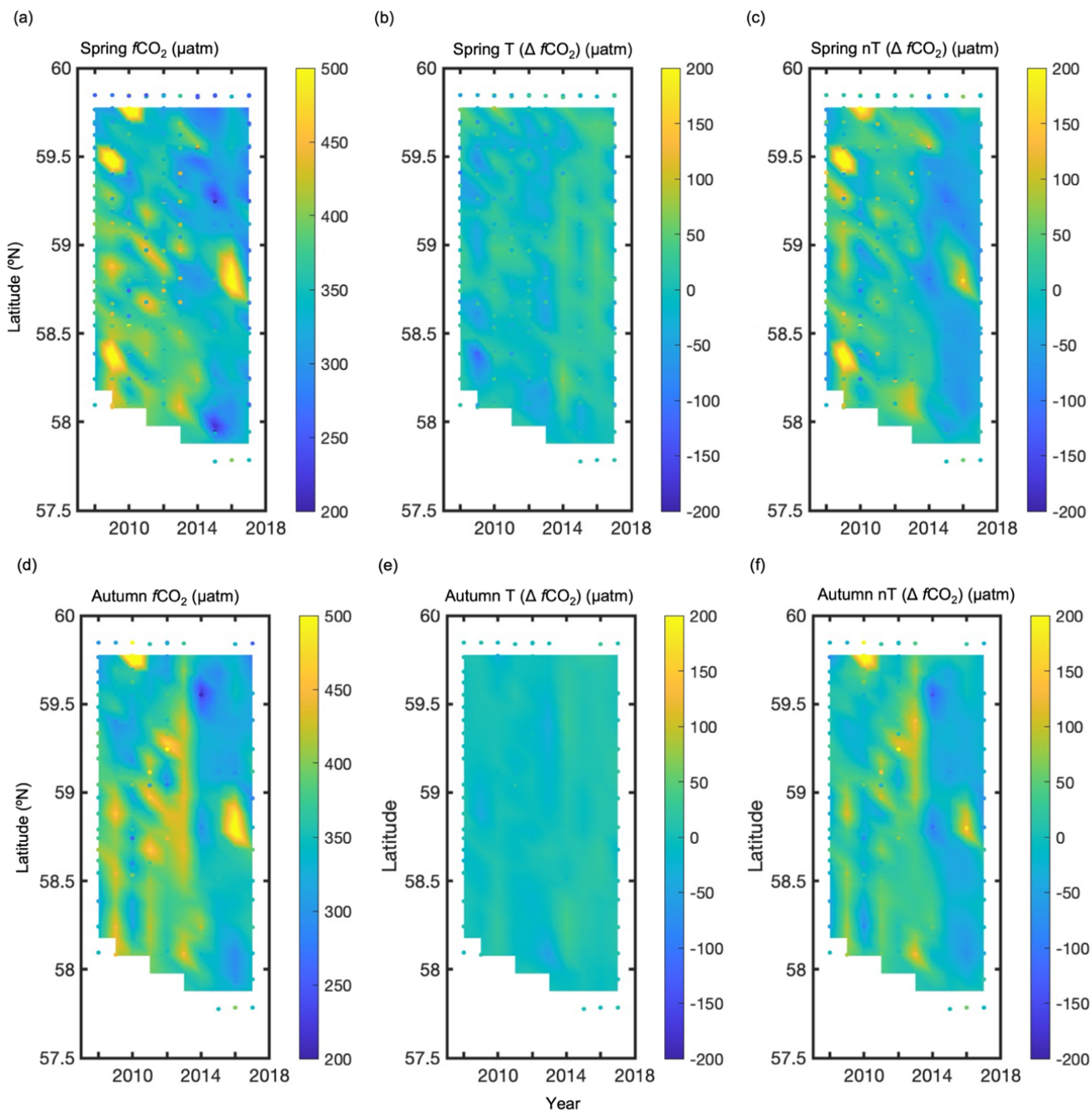
Fig. 6: The fugacity of carbon dioxide (*f*CO₂) is impacted by sea surface temperature (T, Eq 3) and other non–thermal processes (nT, Eq 4). Panels show the upper 50 m of the water column average along the GAK Line transect

from 2008 to 2017 for the a) spring fCO$_2$, b) thermally driven spring fCO$_2$ anomaly [T (Δ fCO$_2$)], c) non–thermal spring fCO$_2$ anomaly [nT (Δ fCO$_2$)], d) autumn fCO$_2$, e) autumn T (Δ fCO$_2$), and f) autumn nT (Δ fCO$_2$).

360   condition the system for weaker spring phytoplankton blooms, either by weaker nutrient replenishment or a change in the phenology of the spring phytoplankton bloom to groups that favor more stratified conditions. Such a state could lead to a weaker and shallower extent of undersaturated surface water with respect to the atmosphere, which then may be easily mixed by episodic wind forcing and lead to the observed fCO$_2$ anomalies. The relationship between the magnitude and frequency of these high fCO$_2$ events, the relaxation of downwelling, and influences on primary productivity requires additional

365   investigation.

3.2 Spatiotemporal trends of CO$_2$

In addition to showing the climatological average spring and fall modes of fCO$_2$ variability, the time–series component of this dataset can also be used to understand the CO$_2$ sink changes over time. In Fig. 7, we split the data into three regional components to show emerging trends in the upper 50 m of different sub–regions of the Seward Line (Fig. 1): nearshore (GAK1–

370   2), middle (GAK3–7), and offshore (GAK8–15). If the surface CO$_2$ increases have been slower than in the atmosphere, this region has been a decreasing CO$_2$ sink during the studied period. Sutton et al. (2019) has reported the Time of Emergence (TOE) of anthropogenic CO$_2$ change depends on the internal variability, which was generally >20 years in coastal regions. Therefore, we acknowledge that the temporal span of these observations is from 2008 to 2017, which may not be sufficient to represent the long–term anthropogenic trends. Indeed, the CO$_2$ trend was insignificant in the nearshore regions in both spring

375   and autumn because of the high interannual variability (Fig. 7). While the anthropogenic CO$_2$ trend did not emerge from the short record in autumn or nearshore subregions, we did find significant variability in the middle and offshore subregions: the surface CO$_2$ has been significantly decreased in the spring. As discussed with Fig. 6b, the influence of temperature anomalies on the fCO$_2$ anomaly is minor compared to nT(ΔfCO$_2$), so the consistent T cannot explain the decreasing fCO$_2$ trend: enhanced primary productivity should support the lower surface fCO$_2$ (~250 µatm) in nearshore and offshore regions after 2014. The

380   increasing primary productivity made this area a rising carbon sink in spring after 2014. However, there is not sufficient information in this dataset to confirm this hypothesis. Sampling in May and September does not sufficiently bracket the spring bloom and is too long for the reliable calculation of seasonal net community production from DIC or nutrient measurements based on best practices (e.g., Mathis et al. 2009). Combining the data shown here with moored datasets, such as from GAKOA (Monacci et al., 2022), and remotely sensed biological parameters, such as chlorophyll, may be a fruitful line of future enquiry.

385
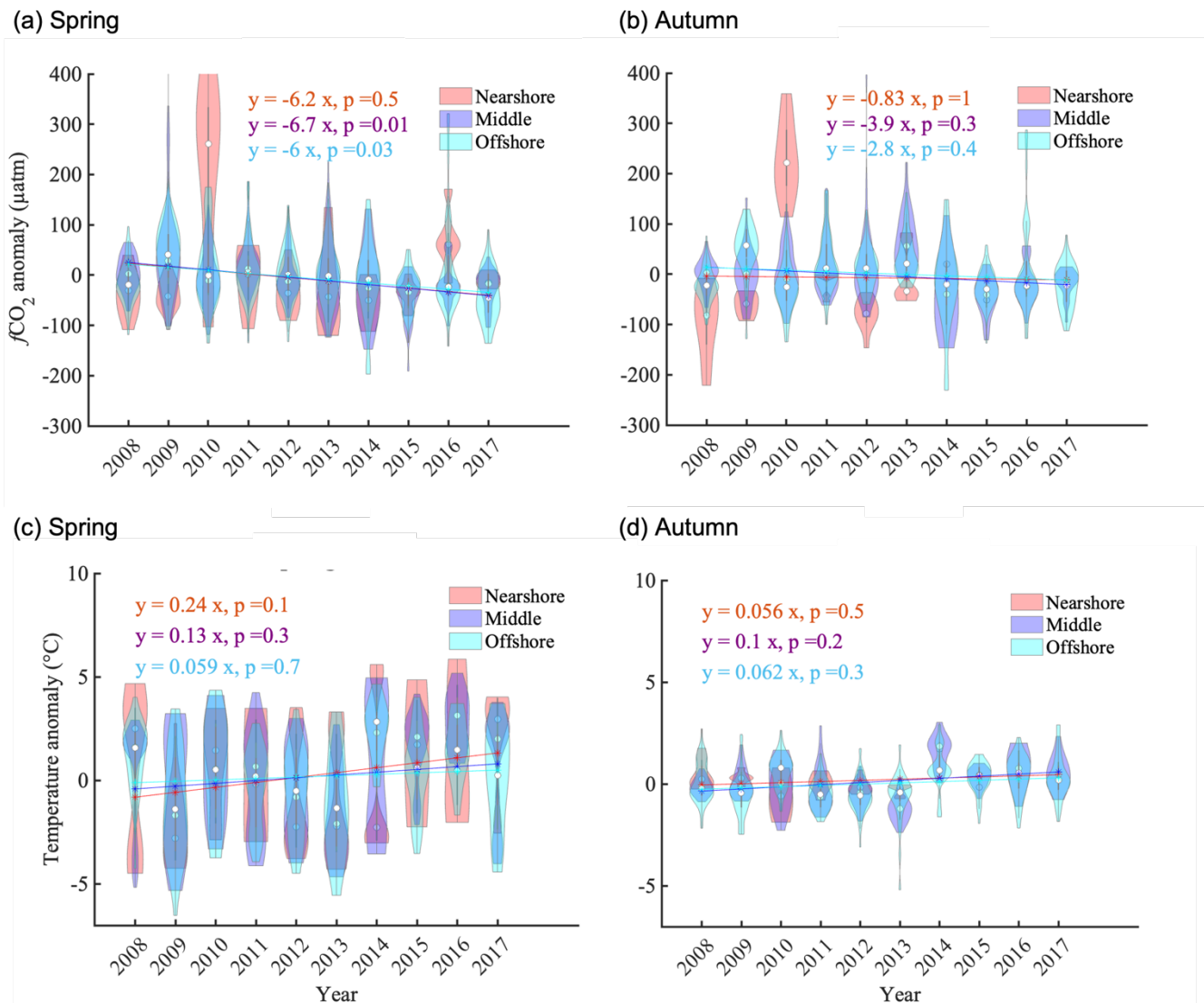
Fig. 7: Regional (nearshore, middle, offshore) violin plots of the upper 50 m fCO_2 and temperature anomaly for spring (a and c) and autumn (b and d). Seward Line stations (Fig. 1) are defined in regions: nearshore (GAK1–2), middle (GAK3–7), and offshore (GAK8–15).

390   **4 Data availability**

The digital object identifier (DOI) for this merged data product is https://doi.org/10.25921/x9sg–9b08 (Monacci et al., 2023). Users looking to access marine carbonate parameter data for the GAK Line that have been designated as good (QF = 2), should consider using this data product. The cruise–level DOIs listed in Table 1 are archived at the National Oceanic and Atmospheric Administration (NOAA) National Centers for Environmental Information (NCEI) (Monacci et al., 2020a–j).

395   These data can also be accessed from the NOAA NCEI Ocean Carbon and Acidification Data System (OCADS) project page: Seward Line Cruises 2008–2017 www.ncei.noaa.gov/access/ocean-carbon-acidification-data-system/oceans/Coastal/seward.html. Users interested in all available data should use the cruise–level data at NCEI (Table 1). Users should also be aware that the GAK Line was visited during the NOAA Ship *Ronald H. Brown* cruise RB1504 (EXPOCODE 33RO20150713) in July 2015. The RB1504 cruise was funded by the NOAA Ocean Acidification Program

400   and data are archived under the DOI https://doi.org/10.25921/dey6-9h45 (Cross et al., 2019).

Data collected during 2008–2012 have been used by Shake (2011) to describe seasonal variability, Evans and Mathis (2013) to determine the Gulf of Alaska as a CO_2 sink, Evans et al. (2013) to develop a regression modeling approach to understand variability, and Hauri et al. (2020) and Siedlecki et al. (2017) to validate regional models. The cruise–level data sets (Table 1)

405   include observations from the western PWS (Fig. 1) but are not included in this merged data product for the GAK Line. Carbonate system data collected in PWS on May and September cruises from 2009 to 2012 were reported in Evans et al. (2014) and Cai et al. (2021). The datasets were not publicly archived at the time of these publications and future uses and references should include the appropriate dataset citations (Monacci et al., 2020a–j). There continues to be a shortage of dataset citations in publications (Vannan et al., 2020), and this data product is direct proof of our support to make data accessible, usable, and

410   citable. We ask users to invite collaboration with the scientific investigators on these datasets as they can provide additional insight. Citation and collaboration are not only good practice but will promote sharing of data and advancing accessibility.

5 Conclusion

This data product provides a distinct data set for users interested in the NGA ecosystem, coastal carbon dynamics, ocean acidification, biogeochemical cycling, and ocean change. The data product can be used to explore natural environmental

415   variability on the physical system and their impacts on marine carbonate parameters. Our examples provide assessments of seasonal, interannual, and regional differences. This data product's timespan is too short to explore the rate of anthropogenic CO_2 absorption, though there are sustained observations in the region using a moored autonomous pCO$_2$ (MAPCO2^{TM}, Sutton et al., 2019) system and through the National Science Foundation's Northern Gulf of Alaska Long–Term Ecological Research program (NGA–LTER). Ocean time–series allow us to understand long–term change and can be an important tool

420   in developing predictions and solutions to continued anthropogenic perturbations. As the global economy turns to the ocean for additional CO_2 sequestration in marine carbon dioxide removal (mCDR) methods, our reliance on time–series sites for our calculations are likely to expand. This data product fills a large gap in the publicly accessible inorganic carbon measurements for a subarctic environment. While our efforts have fallen short of some best practices (e.g., discrete salinity and nutrient measurements) outlined in GLODAPv2 (Olsen et al., 2016), we feel our carbonate parameter measurements are

425   consistent with the OA community goals and standards.

Author contributions

NMM, JNC, WE, and HW contributed to writing and editing. NMM prepared the manuscript and is responsible for the data management, archival, and updates. NMM, JNC, and WE conducted the data QC and error analysis. HW and JNC produced the controls on CO_2. JTM initiated the SL OA program. JNC and JTM were PIs on grants awarded. NMM and WE participated in field work.

Competing Interests

The authors declare that they have no competing interests.

Acknowledgements

We acknowledge and respect that the University of Alaska Fairbanks Troth Yeddha' campus is located on the current, traditional, and ancestral homelands of the Dene people of the lower Tanana Valley and that our study area encompasses the current, traditional, and ancestral region of the Sugpiaq and Alutiiq people. With this acknowledgement, we recognize Indigenous sovereignty and past and current experiences. This work would not have been possible without support from the crew of the USFWS R/V *Tiĝlax̂*. We acknowledge our co–contributors to the 10, unique datasets produced from 20 research cruises including Seth Danielson, Russel Hopcroft, Calvin Mordy, Daniel Naber, Kristen Shake, Katherine Trahanovsky, Thomas Weingartner, Terry Whitledge, and Eric Wisegarver. We thank the Alaska Ocean Observing System under NOAA awards A08NOS4730406, NA11NOS0120020, and NA16NOS0120027 for financial support of the discrete inorganic carbon analyses and the Exxon Valdez Oil Spill Trustee Council, Gulf Watch Alaska, and the North Pacific Research Board for financial support of the research cruises. This manuscript is PMEL contribution number 5508; thank you to Dr. Simone Alin for the internal review.

References

Andrade, J. F., Hurst, T. P., and Miller, J. A.: Behavioral responses of a coastal flatfish to predation–associated cues and elevated CO_2, Journal of Sea Research, 140, 11–21, https://doi.org/10.1016/j.seares.2018.06.013, 2018.

Armstrong, F. A. J., Stearns, C. R., and Strickland, J. D. H.: The measurement of upwelling and subsequent biological process by means of the Technicon Autoanalyzer® and associated equipment, Deep Sea Research and Oceanographic Abstracts, 14, 381–389, https://doi.org/10.1016/0011-7471(67)90082-4, 1967.

Bakun, A.: Coastal upwelling indices, west coast of North America, 1946–71, Technical Report, 1973.

Bakun, A.: Daily and Weekly Upwelling Indices, West Coast of North America, 1967–73, Technical Report, 1975.

Barton, A., Hales, B., Waldbusser, G. G., Langdon, C., and Feely, R. A.: The Pacific oyster, *Crassostrea gigas*, shows negative correlation to naturally elevated carbon dioxide levels: Implications for near–term ocean acidification effects, Limnology and Oceanography, 57, 698–710, https://doi.org/10.4319/lo.2012.57.3.0698, 2012.

Bates, N. R., Orchowska, M. I., Garley, R., and Mathis, J. T.: Summertime calcium carbonate undersaturation in shelf waters of the western Arctic Ocean – how biological processes exacerbate the impact of ocean acidification, Biogeosciences, 10, 5281–5309, https://doi.org/10.5194/bg-10-5281-2013, 2013.

Bechmann, R. K., Taban, I. C., Westerlund, S., Godal, B. F., Arnberg, M., Vingen, S., Ingvarsdottir, A., and Baussant, T.: Effects of Ocean Acidification on Early Life Stages of Shrimp (*Pandalus borealis*) and Mussel (*Mytilus edulis*), Journal of Toxicology and Environmental Health, Part A, 74, 424–438, https://doi.org/10.1080/15287394.2011.550460, 2011.

Bednaršek, N., Tarling, G. A., Bakker, D. C. E., Fielding, S., Jones, E. M., Venables, H. J., Ward, P., Kuzirian, A., Lézé, B., Feely, R. A., and Murphy, E. J.: Extensive dissolution of live pteropods in the Southern Ocean, Nature Geoscience, 5, 881–885, https://doi.org/10.1038/ngeo1635, 2012.

Bednaršek, N., Feely, R. A., Reum, J. C. P., Peterson, B., Menkel, J., Alin, S. R., and Hales, B.: Limacina helicina shell dissolution as an indicator of declining habitat suitability owing to ocean acidification in the California Current Ecosystem, Proceedings of the Royal Society B: Biological Sciences, 281, 20140123, http://dx.doi.org/10.1098/rspb.2014.0123, 2014.

Burton, J. D., Leatherland, T. M., And Liss, P. S.: The Reactivity of Dissolved Silicon in Some Natural Waters, Limnology and Oceanography, 15, 473–476, https://doi.org/10.4319/lo.1970.15.3.0473, 1970.

Byrne, R. H., Mecking, S., Feely, R. A., and Liu, X.: Direct observations of basin–wide acidification of the North Pacific Ocean, Geophysical Research Letters, 37, https://doi.org/10.1029/2009GL040999, 2010.

Cai, W.–J., Feely, R. A., Testa, J. M., Li, M., Evans, W., Alin, S. R., Xu, Y.–Y., Pelletier, G., Ahmed, A., Greeley, D. J., Newton, J. A., and Bednaršek, N.: Natural and Anthropogenic Drivers of Acidification in Large Estuaries, Annual Review of Marine Science, 13, 23–55, https://doi.org/10.1146/annurev-marine-010419-011004, 2021.

Carpenter, J. H.: The Accuracy of The Winkler Method for Dissolved Oxygen Analysis, Limnology and Oceanography, 10, 135–140, 1965.

Childers, A. R., Whitledge, T. E., and Stockwell, D. A.: Seasonal and interannual variability in the distribution of nutrients and chlorophyll a across the Gulf of Alaska shelf: 1998–2000, Deep Sea Research Part II: Topical Studies in Oceanography, 52, 193–216, https://doi.org/10.1016/j.dsr2.2004.09.018, 2005.

Comeau, S., Jeffree, R., Teyssié, J.–L., and Gattuso, J.–P.: Response of the Arctic Pteropod *Limacina helicina* to Projected Future Environmental Conditions, PLOS ONE, 5, e11362, https://doi.org/10.1371/journal.pone.0011362, 2010.

Cooley, S. R. and Doney, S. C.: Anticipating ocean acidification's economic consequences for commercial fisheries, Environmental Research Letters, 4, 024007, https://dx.doi.org/10.1088/1748-9326/4/2/024007, 2009.

485   Cross, J. N., Mathis, J. T., Bates, N. R., and Byrne, R. H.: Conservative and non–conservative variations of total alkalinity on the southeastern Bering Sea shelf, Marine Chemistry, 154, 100–112, https://doi.org/10.1016/j.marchem.2013.05.012, 2013.

Cross, J. N., Mathis, J. T., Pickart, R. S., and Bates, N. R.: Formation and transport of corrosive water in the Pacific Arctic region, Deep Sea Research Part II: Topical Studies in Oceanography, 152, 67–81,

490   https://doi.org/10.1016/j.dsr2.2018.05.020, 2018.

Cross, J. N., Monacci, N. M., Mathis, J. T.: Dissolved inorganic carbon (DIC), total alkalinity and other hydrographic and chemical variables collected from discrete samples and profile observations during NOAA Ship Ronald H. Brown cruise RB1504 (EXPOCODE 33RO20150713) in the Gulf of Alaska from 2015–07–13 to 2015–07–31 (NCEI Accession 0201748). NOAA National Centers for Environmental Information. Dataset. https://doi.org/10.25921/dey6-9h45, 2019.

495   Dickson, A. G.: Thermodynamics of the dissociation of boric acid in synthetic seawater from 273.15 to 318.15 K, Deep Sea Research Part A. Oceanographic Research Papers, 37, 755–766, https://doi.org/10.1016/0198-0149(90)90004-F, 1990.

Dillon, W. D. N., Dillingham, P. W., Currie, K. I., and McGraw, C. M.: Inclusion of uncertainty in the calcium–salinity relationship improves estimates of ocean acidification monitoring data quality, Marine Chemistry, 226, 103872, https://doi.org/10.1016/j.marchem.2020.103872, 2020.

500   Dore, J. E., Lukas, R., Sadler, D. W., Church, M. J., and Karl, D. M.: Physical and biogeochemical modulation of ocean acidification in the central North Pacific, Proceedings of the National Academy of Sciences, 106, 12235–12240, https://www.pnas.org/doi/abs/10.1073/pnas.0906044106, 2009.

Evans, W. and Mathis, J. T.: The Gulf of Alaska coastal ocean as an atmospheric CO_2 sink, Continental Shelf Research, 65, 52–63, https://doi.org/10.1016/j.csr.2013.06.013, 2013.

505   Evans, W., Mathis, J. T., Winsor, P., Statscewich, H., and Whitledge, T. E.: A regression modeling approach for studying carbonate system variability in the northern Gulf of Alaska, Journal of Geophysical Research: Oceans, 118, 476–489, https://doi.org/10.1029/2012JC008246, 2013.

Evans, W., Mathis, J. T., and Cross, J. N.: Calcium carbonate corrosivity in an Alaskan inland sea, Biogeosciences, 11, 365–379, https://doi.org/10.5194/bg-11-365-2014, 2014.

510   Feely, R. A., Sabine, C. L., Lee, K., Berelson, W., Kleypas, J., Fabry, V. J., and Millero, F. J.: Impact of Anthropogenic CO_2 on the $CaCO_3$ System in the Oceans, Science, 305, 362–366, https://doi.org/10.1126/science.1097329, 2004.

Feely, R. A., Sabine, C. L., Hernandez–Ayon, J. M., Ianson, D., and Hales, B.: Evidence for Upwelling of Corrosive "Acidified" Water onto the Continental Shelf, Science, 320, 1490–1492, https://doi.org/10.1126/science.1155676, 2008.

Feely, R. A. D., Scott C., Cooley, Sarah R.: Ocean Acidification: Present Conditions and Future Changes in a High–CO_2

515   World, Oceanography, 22, https://doi.org/10.5670/oceanog.2009.95, 2009.

Feely, R. A., Okazaki, R. R., Cai, W.–J., Bednaršek, N., Alin, S. R., Byrne, R. H., and Fassbender, A.: The combined effects of acidification and hypoxia on pH and aragonite saturation in the coastal waters of the California current ecosystem and the northern Gulf of Mexico, Continental Shelf Research, 152, 50–60, https://doi.org/10.1016/j.csr.2017.11.002, 2018.

Fissel, B., Dalton, M., Garber–Yonts, B., Haynie, A., Kasperski, S., Lee, J., Lew, D., Seung, C., Sparks, K., Szymkowiak, M., and Wise, S.: Stock assessment and fishery evaluation report for the groundfish fisheries of the Gulf of Alaska and Bering Sea / Aleutian Islands area: Economic Status of the Groundfish fisheries off Alaska, 2019, Alaska Fisheries Science Center, National Marine Fisheries Service, National Oceanic and Atmospheric Administration, 2021.

Friedlingstein, P., O'Sullivan, M., Jones, M. W., Andrew, R. M., Gregor, L., Hauck, J., Le Quéré, C., Luijkx, I. T., Olsen, A., Peters, G. P., Peters, W., Pongratz, J., Schwingshackl, C., Sitch, S., Canadell, J. G., Ciais, P., Jackson, R. B., Alin, S. R., Alkama, R., Arneth, A., Arora, V. K., Bates, N. R., Becker, M., Bellouin, N., Bittig, H. C., Bopp, L., Chevallier, F., Chini, L. P., Cronin, M., Evans, W., Falk, S., Feely, R. A., Gasser, T., Gehlen, M., Gkritzalis, T., Gloege, L., Grassi, G., Gruber, N., Gürses, Ö., Harris, I., Hefner, M., Houghton, R. A., Hurtt, G. C., Iida, Y., Ilyina, T., Jain, A. K., Jersild, A., Kadono, K., Kato, E., Kennedy, D., Klein Goldewijk, K., Knauer, J., Korsbakken, J. I., Landschützer, P., Lefèvre, N., Lindsay, K., Liu, J., Liu, Z., Marland, G., Mayot, N., McGrath, M. J., Metzl, N., Monacci, N. M., Munro, D. R., Nakaoka, S. I., Niwa, Y., O'Brien, K., Ono, T., Palmer, P. I., Pan, N., Pierrot, D., Pocock, K., Poulter, B., Resplandy, L., Robertson, E., Rödenbeck, C., Rodriguez, C., Rosan, T. M., Schwinger, J., Séférian, R., Shutler, J. D., Skjelvan, I., Steinhoff, T., Sun, Q., Sutton, A. J., Sweeney, C., Takao, S., Tanhua, T., Tans, P. P., Tian, X., Tian, H., Tilbrook, B., Tsujino, H., Tubiello, F., van der Werf, G. R., Walker, A. P., Wanninkhof, R., Whitehead, C., Willstrand Wranne, A., Wright, R., Yuan, W., Yue, C., Yue, X., Zaehle, S., Zeng, J., and Zheng, B.: Global Carbon Budget 2022, Earth Syst. Sci. Data, 14, 4811–4900, https://doi.org/10.5194/essd-14-4811-2022, 2022.

Frisch, L. C., Mathis, J. T., Kettle, N. P., and Trainor, S. F.: Gauging perceptions of ocean acidification in Alaska, Marine Policy, 53, 101–110, https://doi.org/10.1016/j.marpol.2014.11.022, 2015.

Gordon, L. I., Jennings Jr., J. C., Ross, A. A., and Krest, J. M.: A Suggested Protocol for Continuous Flow Automated Analysis of Seawater Nutrients (Phosphate, Nitrate, Nitrite and Silicic Acid) in the WOCE Hydrographic Program and the Joint Global Ocean Fluxes Study, in: WOCE Hydrographic Program Office, Methods Manual WHPO 91–1, Oregon State University Technical Report, 93–1, 1993.

Gouretski, V. V. and Jancke, K.: Systematic errors as the cause for an apparent deep water property variability: global analysis of the WOCE and historical hydrographic data, Progress in Oceanography, 48, 337–402, https://doi.org/10.1016/S0079-6611(00)00049-5, 2000.

Gruber, N., Bakker, D. C. E., DeVries, T., Gregor, L., Hauck, J., Landschützer, P., McKinley, G. A., and Müller, J. D.: Trends and variability in the ocean carbon sink, Nature Reviews Earth & Environment, 4, 119–134, https://doi.org/10.1038/s43017-022-00381-x, 2023.

Hauri, C., Schultz, C., Hedstrom, K., Danielson, S., Irving, B., Doney, S. C., Dussin, R., Curchitser, E. N., Hill, D. F., and Stock, C. A.: A regional hindcast model simulating ecosystem dynamics, inorganic carbon chemistry, and ocean acidification in the Gulf of Alaska, Biogeosciences, 17, 3837–3857, https://doi.org/10.5194/bg-17-3837-2020, 2020.

Hurst, T. P., Fernandez, E. R., Mathis, J. T., Miller, J. A., Stinson, C. M., and Ahgeak, E. F.: Resiliency of juvenile walleye pollock to projected levels of ocean acidification, Aquatic Biology, 17, 247–259, https://doi.org/10.3354/ab00483, 2012.

Hurst, T. P., Fernandez, E. R., and Mathis, J. T.: Effects of ocean acidification on hatch size and larval growth of walleye pollock (*Theragra chalcogramma*), ICES Journal of Marine Science, 70, 812–822, https://doi.org/10.1093/icesjms/fst053, 2013.

Hurst, T. P., Copeman, L. A., Haines, S. A., Meredith, S. D., Daniels, K., and Hubbard, K. M.: Elevated CO_2 alters behavior, growth, and lipid composition of Pacific cod larvae, Marine Environmental Research, 145, 52–65, https://doi.org/10.1016/j.marenvres.2019.02.004, 2019.

Jacox, M. G., Edwards, C. A., Hazen, E. L., and Bograd, S. J.: Coastal Upwelling Revisited: Ekman, Bakun, and Improved Upwelling Indices for the U.S. West Coast, Journal of Geophysical Research: Oceans, 123, 7332–7350, https://doi.org/10.1029/2018JC014187, 2018.

Jiang, L.–Q., Carter, B. R., Feely, R. A., Lauvset, S. K., and Olsen, A.: Surface ocean pH and buffer capacity: past, present and future, Scientific Reports, 9, 18624, https://doi.org/10.1038/s41598-019-55039-4, 2019.

Jiang, L. Q., Feely, R. A., Wanninkhof, R., Greeley, D., Barbero, L., Alin, S., Carter, B. R., Pierrot, D., Featherstone, C., Hooper, J., Melrose, C., Monacci, N., Sharp, J. D., Shellito, S., Xu, Y. Y., Kozyr, A., Byrne, R. H., Cai, W. J., Cross, J., Johnson, G. C., Hales, B., Langdon, C., Mathis, J., Salisbury, J., and Townsend, D. W.: Coastal Ocean Data Analysis Product in North America (CODAP–NA) – an internally consistent data product for discrete inorganic carbon, oxygen, and nutrients on the North American ocean margins, Earth Syst. Sci. Data, 13, 2777–2799, https://doi.org/10.5194/essd-13-2777-2021, 2021.

Jiang, L.–Q., Pierrot, D., Wanninkhof, R., Feely, R. A., Tilbrook, B., Alin, S., Barbero, L., Byrne, R. H., Carter, B. R., Dickson, A. G., Gattuso, J.–P., Greeley, D., Hoppema, M., Humphreys, M. P., Karstensen, J., Lange, N., Lauvset, S. K., Lewis, E. R., Olsen, A., Pérez, F. F., Sabine, C., Sharp, J. D., Tanhua, T., Trull, T. W., Velo, A., Allegra, A. J., Barker, P., Burger, E., Cai, W.–J., Chen, C.–T. A., Cross, J., Garcia, H., Hernandez–Ayon, J. M., Hu, X., Kozyr, A., Langdon, C., Lee, K., Salisbury, J., Wang, Z. A., and Xue, L.: Best Practice Data Standards for Discrete Chemical Oceanographic Observations, Frontiers in Marine Science, 8, https://doi.org/10.3389/fmars.2021.705638, 2022.

Johnson, G. C., Robbins, P. E., and Hufford, G. E.: Systematic Adjustments of Hydrographic Sections for Internal Consistency, Journal of Atmospheric and Oceanic Technology, 18, 1234–1244, https://doi.org/10.1175/1520-0426(2001)018%3C1234:SAOHSF%3E2.0.CO;2, 2001.

Ladd, C., Cheng, W., and Salo, S.: Gap winds and their effects on regional oceanography Part II: Kodiak Island, Alaska, Deep Sea Research Part II: Topical Studies in Oceanography, 132, 54–67, https://doi.org/10.1016/j.dsr2.2015.08.005, 2016.

Langdon, C.: Determination of Dissolved Oxygen in Seawater by Winkler Titration Using The Amperometric Technique, 18, https://doi.org/10.25607/OBP-1350, 2010.

Lauvset, S. K., Lange, N., Tanhua, T., Bittig, H. C., Olsen, A., Kozyr, A., Alin, S., Álvarez, M., Azetsu–Scott, K., Barbero, L., Becker, S., Brown, P. J., Carter, B. R., da Cunha, L. C., Feely, R. A., Hoppema, M., Humphreys, M. P., Ishii, M., Jeansson, E., Jiang, L. Q., Jones, S. D., Lo Monaco, C., Murata, A., Müller, J. D., Pérez, F. F., Pfeil, B., Schirnick, C.,

Steinfeldt, R., Suzuki, T., Tilbrook, B., Ulfsbo, A., Velo, A., Woosley, R. J., and Key, R. M.: GLODAPv2.2022: the latest version of the global interior ocean biogeochemical data product, Earth Syst. Sci. Data, 14, 5543–5572, https://doi.org/10.5194/essd-14-5543-2022, 2022.

590   Long, C. W., Swiney, K. M., and Foy, R. J.: Effects of ocean acidification on the embryos and larvae of red king crab, *Paralithodes camtschaticus*, Marine Pollution Bulletin, 69, 38–47, https://doi.org/10.1016/j.marpolbul.2013.01.011, 2013.

Macdonald, R. W., McLaughlin, F. A., and Wong, C. S.: The storage of reactive silicate samples by freezing, Limnology and Oceanography, 31, 1139–1142, https://doi.org/10.4319/lo.1986.31.5.1139, 1986.

595   Mathis, J. T., Bates, N. R., Hansell, D. A., and Babila, T.: Net community production in the northeastern Chukchi Sea, Deep Sea Research Part II: Topical Studies in Oceanography, 56, 1213–1222, https://doi.org/10.1016/j.dsr2.2008.10.017, 2009.

Mathis, J. T., Cross, J. N., and Bates, N. R.: The role of ocean acidification in systemic carbonate mineral suppression in the Bering Sea, Geophysical Research Letters, 38, https://doi.org/10.1029/2011GL048884, 2011a.

600   Mathis, J. T., Cross, J. N., and Bates, N. R.: Coupling primary production and terrestrial runoff to ocean acidification and carbonate mineral suppression in the eastern Bering Sea, Journal of Geophysical Research: Oceans, 116, https://doi.org/10.1029/2010JC006453, 2011b.

Mathis, J. T., Pickart, R. S., Byrne, R. H., McNeil, C. L., Moore, G. W. K., Juranek, L. W., Liu, X., Ma, J., Easley, R. A., Elliot, M. M., Cross, J. N., Reisdorph, S. C., Bahr, F., Morison, J., Lichendorf, T., and Feely, R. A.: Storm–induced

605   upwelling of high pCO$_2$ waters onto the continental shelf of the western Arctic Ocean and implications for carbonate mineral saturation states, Geophysical Research Letters, 39, https://doi.org/10.1029/2012GL051574, 2012.

Mathis, J. T., Cross, J. N., Monacci, N., Feely, R. A., and Stabeno, P.: Evidence of prolonged aragonite undersaturations in the bottom waters of the southern Bering Sea shelf from autonomous sensors, Deep Sea Research Part II: Topical Studies in Oceanography, 109, 125–133, https://doi.org/10.1016/j.dsr2.2013.07.019, 2014.

610   Mathis, J. T., Cooley, S. R., Lucey, N., Colt, S., Ekstrom, J., Hurst, T., Hauri, C., Evans, W., Cross, J. N., and Feely, R. A.: Ocean acidification risk assessment for Alaska's fishery sector, Progress in Oceanography, 136, 71–91, https://doi.org/10.1016/j.pocean.2014.07.001, 2015.

Millero, F., Graham, T., Huang, F., Bustos–Serrano, H., and Pierrot, D.: Dissociation constants of carbonic acid in seawater as a function of salinity and temperature, Marine Chemistry, 100, 80–94,

615   https://doi.org/10.1016/j.marchem.2005.12.001, 2006.

Monacci, N. M., Cross, J. N., Mathis, J. T., Hopcroft, R.R., Naber, D., Shake, K. L., Trahanovsky, K., Whitledge, T. E. Discrete profile measurements of dissolved inorganic carbon (DIC), total alkalinity (TA), temperature, salinity, oxygen, nutrients and other parameters during the R/V Tiĝlax̂ Seward Line cruises TXS08 and TXF08 (EXPOCODEs: 33A020080502 and 33A020080913) in the Gulf of Alaska, North Pacific Ocean from 2008–05–02 to 2008–09–16

620   (NCEI Accession 0209723). NOAA National Centers for Environmental Information. Dataset.
https://doi.org/10.25921/44kh-zb66, 2020a.

Monacci, N. M., Cross, J. N., Mathis, J. T., Hopcroft, R.R., Naber, D., Shake, K. L., Trahanovsky, K., Whitledge, T. E.
Discrete profile measurements of dissolved inorganic carbon (DIC), total alkalinity (TA), temperature, salinity, oxygen,
nutrients and other parameters during the R/V Tiĝlax̂ Seward Line cruises TXS09 and TXF09 (EXPOCODEs:
625   33A020090503 and 33A020090914) in the Gulf of Alaska, North Pacific Ocean from 2009–05–03 to 2009–09–19
(NCEI Accession 0210032). NOAA National Centers for Environmental Information. Dataset.
https://doi.org/10.25921/n43y-9r47, 2020b.

Monacci, N. M., Cross, J. N., Mathis, J. T., Hopcroft, R.R., Naber, D., Shake, K. L., Trahanovsky, K., Whitledge, T. E.
Discrete profile measurements of dissolved inorganic carbon (DIC), total alkalinity (TA), temperature, salinity, oxygen,
630   nutrients and other parameters during the R/V Norseman II and R/V Tiĝlax̂ Seward Line cruises N2S10 and TXF10
(EXPOCODEs: 32QO20100503 and 33A020100914) in the Gulf of Alaska, North Pacific Ocean from 2010–05–03 to
2010–09–18 (NCEI Accession 0210125). NOAA National Centers for Environmental Information. Dataset.
https://doi.org/10.25921/avxr-m571, 2020c.

Monacci, N. M., Cross, J. N., Mathis, J. T., Hopcroft, R. R., Mordy, C., Shake, K. L., Wisegarver, E. Discrete profile
635   measurements of dissolved inorganic carbon (DIC), total alkalinity (TA), temperature, salinity, oxygen, nutrients and
Delta Oxygen–18 during the R/V Tiĝlax̂ Seward Line cruises TXS11 and TXF11 (EXPOCODEs: 33A020110506 and
33A020110915) in the Gulf of Alaska, North Pacific Ocean from 2011–05–06 to 2011–09–19 (NCEI Accession
0210127). NOAA National Centers for Environmental Information. Dataset. https://doi.org/10.25921/07yn-b044, 2020d.

Monacci, N. M., Cross, J. N., Mathis, J. T., Evans, W., Hopcroft, R.R., Naber, D., Shake, K. L., Trahanovsky, K., Whitledge,
640   T. E. Discrete profile measurements of dissolved inorganic carbon (DIC), total alkalinity (TA), temperature, salinity,
oxygen, nutrients and Delta Oxygen–18 during the R/V Tiĝlax̂ Seward Line cruises TXS12 and TXF12 (EXPOCODEs:
33A020120503 and 33A020120913) in the Gulf of Alaska, North Pacific Ocean from 2012–05–03 to 2012–09–18
(NCEI Accession 0210221). NOAA National Centers for Environmental Information. Dataset.
https://doi.org/10.25921/mttc-gc63, 2020e.

645   Monacci, N. M., Cross, J. N., Hopcroft, R. R., Mathis, J. T. Discrete profile measurements of dissolved inorganic carbon
(DIC), total alkalinity (TA), temperature, salinity, oxygen, nutrients and Delta Oxygen–18 during the R/V Tiĝlax̂ Seward
Line cruises TXS13 and TXF13 (EXPOCODEs: 33A020130427 and 33A020130914) in the Gulf of Alaska, North
Pacific Ocean from 2013–04–27 to 2013–09–26 (NCEI Accession 0210222). NOAA National Centers for
Environmental Information. Dataset. https://doi.org/10.25921/n5dy-h455, 2020f.

650   Monacci, N. M., Cross, J. N., Hopcroft, R. R., Mathis, J. T. Discrete profile measurements of dissolved inorganic carbon
(DIC), total alkalinity (TA), temperature, salinity, oxygen, nutrients and Delta Oxygen–18 during the R/V Tiĝlax̂ Seward
Line cruises TXS14 and TXF14 (EXPOCODEs: 33A020140503 and 33A020140913) in the Gulf of Alaska, North

Pacific Ocean from 2014–05–03 to 2014–09–19 (NCEI Accession 0210223). NOAA National Centers for Environmental Information. Dataset. https://doi.org/10.25921/ke3w-xp11, 2020g.

655 Monacci, N. M., Cross, J. N., Hopcroft, R. R., Mathis, J. T. Discrete profile measurements of dissolved inorganic carbon (DIC), total alkalinity (TA), temperature, salinity, oxygen, nutrients and other parameters during the R/V Tiĝlâx̂ Seward Line cruises TXS15 and TXF15 (EXPOCODEs: 33A020150505 and 33A020150914) in the Gulf of Alaska, North Pacific Ocean from 2015–05–05 to 2015–09–20 (NCEI Accession 0210224). NOAA National Centers for Environmental Information. Dataset. https://doi.org/10.25921/r7kp-0j46, 2020h.

660 Monacci, N. M., Cross, J. N., Hopcroft, R. R., Mathis, J. T. Discrete profile measurements of dissolved inorganic carbon (DIC), total alkalinity (TA), temperature, salinity, oxygen, nutrients and other parameters during the R/V Tiĝlâx̂ Seward Line cruises TXS16 and TXF16 (EXPOCODEs: 33A020160430 and 33A020160915) in the Gulf of Alaska, North Pacific Ocean from 2016–04–30 to 2016–09–20 (NCEI Accession 0210235). NOAA National Centers for Environmental Information. Dataset. https://doi.org/10.25921/ed32-3h29, 2020i.

665 Monacci, N. M., Cross, J. N., Hopcroft, R. R., Mathis, J. T. Discrete profile measurements of dissolved inorganic carbon (DIC), total alkalinity (TA), temperature, salinity, oxygen, nutrients and other parameters during the R/V Tiĝlâx̂ Seward Line cruises TXS17 and TXF17 (EXPOCODEs: 33A020170501 and 33A020170916) in the Gulf of Alaska, North Pacific Ocean from 2017–05–01 to 2017–09–22 (NCEI Accession 0210236). NOAA National Centers for Environmental Information. Dataset. https://doi.org/10.25921/rvm1-vj65, 2020j.

670 Monacci, N.M., Bott, R., Cross, J.N., Maenner–Jones, S., Musielewicz, S., Osborne, J., Sutton, A. High–resolution ocean and atmosphere pCO$_2$ time–series measurements from mooring GAKOA_149W_60N. NOAA National Centers for Environmental Information. Dataset. https://doi.org/10.3334/cdiac/otg.tsm_gakoa_149w_60n, 2022.

Monacci, N. M., Cross, J. N., Danielson, S. L., Evans, W., Hopcroft, R. R., Mathis, J. T., Mordy, C. W., Naber, D. D., Shake, K. L., Trahanovsky, K., Wang, H., Weingartner, T. J., and Whitledge, T. E.: Marine carbonate system discrete profile

675 data from the Gulf of Alaska (GAK) Seward Line cruises between 2008 and 2017 (NCEI Accession 0277034). NOAA National Centers for Environmental Information. Dataset. https://doi.org/10.25921/x9sg-9b08, 2023.

Murphy, J. and Riley, J. P.: A modified single solution method for the determination of phosphate in natural waters, Analytica Chimica Acta, 27, 31–36, https://doi.org/10.1016/S0003-2670(00)88444-5, 1962.

National Marine Fisheries Service (NMFS): Fisheries of the United States, 2020., U.S. Department of Commerce, NOAA,

680 https://www.fisheries.noaa.gov/national/sustainable-fisheries/fisheries-united-states, 2022.

Olsen, A., Key, R. M., van Heuven, S., Lauvset, S. K., Velo, A., Lin, X., Schirnick, C., Kozyr, A., Tanhua, T., Hoppema, M., Jutterström, S., Steinfeldt, R., Jeansson, E., Ishii, M., Pérez, F. F., and Suzuki, T.: The Global Ocean Data Analysis Project version 2 (GLODAPv2) – an internally consistent data product for the world ocean, Earth Syst. Sci. Data, 8, 297–323, https://doi.org/10.5194/essd-8-297-2016, 2016.

685 Olsen, A., Key, R. M., Lauvset, S. K., Kozyr, A., Tanhua, T., Hoppema, M., Ishii, M., Jeansson, E., van Heuven, S. M. A. C., Jutterström, S., Schirnick, C., Steinfeldt, R., Suzuki, T., Lin, X., Velo, A., Pérez, F. F. Global Ocean Data Analysis

Project, Version 2 (GLODAPv2) (NCEI Accession 0162565). Version 2. NOAA National Centers for Environmental Information. Dataset. https://doi.org/10.7289/v5kw5d97, 2017.

Orr, J. C., Epitalon, J. M., and Gattuso, J. P.: Comparison of ten packages that compute ocean carbonate chemistry, Biogeosciences, 12, 1483–1510, https://doi.org/10.5194/bg-12-1483-2015, 2015.

Orr, J. C., Epitalon, J.–M., Dickson, A. G., and Gattuso, J.–P.: Routine uncertainty propagation for the marine carbon dioxide system, Marine Chemistry, 207, 84–107, https://doi.org/10.1016/j.marchem.2018.10.006, 2018.

Punt, A. E., Poljak, D., Dalton, M. G., and Foy, R. J.: Evaluating the impact of ocean acidification on fishery yields and profits: The example of red king crab in Bristol Bay, Ecological Modelling, 285, 39–53, https://doi.org/10.1016/j.ecolmodel.2014.04.017, 2014.

Punt, A. E., Dalton, M. G., Cheng, W., Hermann, A. J., Holsman, K. K., Hurst, T. P., Ianelli, J. N., Kearney, K. A., McGilliard, C. R., Pilcher, D. J., and Véron, M.: Evaluating the impact of climate and demographic variation on future prospects for fish stocks: An application for northern rock sole in Alaska, Deep Sea Research Part II: Topical Studies in Oceanography, 189–190, 104951, https://doi.org/10.1016/j.dsr2.2021.104951, 2021.

Reed, R. K., Schumacher, J. D., and Incze, L. S.: Circulation in Shelikof Strait, Alaska, Journal of Physical Oceanography, 17, 1546–1554, https://doi.org/10.1175/1520-0485(1987)017%3C1546:CISSA%3E2.0.CO;2, 1987.

Reisdorph, S. C. and Mathis, J. T.: The dynamic controls on carbonate mineral saturation states and ocean acidification in a glacially dominated estuary, Estuarine, Coastal and Shelf Science, 144, 8–18, https://doi.org/10.1016/j.ecss.2014.03.018, 2014.

Royer, T. C.: Seasonal variations of waters in the northern Gulf of Alaska, Deep Sea Research and Oceanographic Abstracts, 22, 403–416, https://doi.org/10.1016/0011-7471(75)90062-5, 1975.

Royer, T. C. and Emery, W. J.: Circulation in the Gulf of Alaska, 1981, Deep Sea Research Part A. Oceanographic Research Papers, 34, 1361–1377, https://doi.org/10.1016/0198-0149(87)90132-4, 1987.

Sabine, C. L. and Tanhua, T.: Estimation of Anthropogenic CO_2 Inventories in the Ocean, Annual Review of Marine Science, 2, 175–198, https://doi.org/10.1146/annurev-marine-120308-080947, 2010.

Schwing, F. B., O'Farrell, M., Steger, J., and Baltz, K.: Coastal Upwelling Indices, West Coast of North America, 1946–1995, Technical Report, National Marine Fisheries Service, National Oceanic and Atmospheric Administration, 28, 1996.

Seung, C. K., Dalton, M. G., Punt, A. E., Poljak, D., and Foy, R.: Economic Impacts Of Changes in an Alaska Crab Fishery from Ocean Acidification, Climate Change Economics, 06, 1550017, https://doi.org/10.1142/s2010007815500177, 2015.

Shake, K. L.: Hydrographic controls and seasonal variability on the carbonate system in the Northern Gulf of Alaska, M.S. thesis, College of Fisheries and Oceans Sciences, University of Alaska Fairbanks, Fairbanks, AK USA, 106 pp., 2011.

Sharp, J. D. and Byrne, R. H.: Technical note: Excess alkalinity in carbonate system reference materials, Marine Chemistry, 233, 103965, https://doi.org/10.1016/j.marchem.2021.103965, 2021.

Siedlecki, S. A., Pilcher, D. J., Hermann, A. J., Coyle, K., and Mathis, J.: The Importance of Freshwater to Spatial Variability of Aragonite Saturation State in the Gulf of Alaska, Journal of Geophysical Research: Oceans, 122, 8482–8502, https://doi.org/10.1002/2017JC012791, 2017.

Stabeno, P. J., Bond, N. A., Hermann, A. J., Kachel, N. B., Mordy, C. W., and Overland, J. E.: Meteorology and oceanography of the Northern Gulf of Alaska, Continental Shelf Research, 24, 859–897, https://doi.org/10.1016/j.csr.2004.02.007, 2004.

Sutton, A. J., Feely, R. A., Maenner–Jones, S., Musielwicz, S., Osborne, J., Dietrich, C., Monacci, N., Cross, J., Bott, R., Kozyr, A., Andersson, A. J., Bates, N. R., Cai, W. J., Cronin, M. F., De Carlo, E. H., Hales, B., Howden, S. D., Lee, C. M., Manzello, D. P., McPhaden, M. J., Meléndez, M., Mickett, J. B., Newton, J. A., Noakes, S. E., Noh, J. H., Olafsdottir, S. R., Salisbury, J. E., Send, U., Trull, T. W., Vandemark, D. C., and Weller, R. A.: Autonomous seawater pCO$_2$ and pH time series from 40 surface buoys and the emergence of anthropogenic trends, Earth Syst. Sci. Data, 11, 421–439, https://doi.org/10.5194/essd-11-421-2019, 2019.

Szymkowiak, M. and Steinkruger, A.: Alaska fishers attest to climate change impacts in discourse on resource management under marine heatwaves, Environmental Science & Policy, 140, 261–270, https://doi.org/10.1016/j.envsci.2022.12.019, 2023.

Takahashi, T., Sutherland, S. C., Sweeney, C., Poisson, A., Metzl, N., Tilbrook, B., Bates, N., Wanninkhof, R., Feely, R. A., Sabine, C., Olafsson, J., and Nojiri, Y.: Global sea–air CO$_2$ flux based on climatological surface ocean pCO$_2$, and seasonal biological and temperature effects, Deep Sea Research Part II: Topical Studies in Oceanography, 49, 1601–1622, https://doi.org/10.1016/S0967-0645(02)00003-6, 2002.

Tanhua, T., van Heuven, S., Key, R. M., Velo, A., Olsen, A., and Schirnick, C.: Quality control procedures and methods of the CARINA database, Earth Syst. Sci. Data, 2, 35–49, https://doi.org/10.5194/essd-2-35-2010, 2010.

Uppström, L. R.: The boron/chlorinity ratio of deep–sea water from the Pacific Ocean, Deep Sea Research and Oceanographic Abstracts, 21, 161–162, https://doi.org/10.1016/0011-7471(74)90074-6, 1974.

van Heuven, S., Pierrot, D., Rae, J. W. B., Lewis, E., and Wallace, D. W. R.: MATLAB Program Developed for CO$_2$ System Calculations, Carbon Dioxide Information Analysis Center, Oak Ridge National Laboratory, U.S. Department of Energy [code], https://doi.org/10.3334/CDIAC/otg.CO2SYS_MATLAB_v1.1, 2011.

Vannan, S., Downs, R. R., Meier, W., Wilson, B. E., and Gerasimov, I. V.: Data sets are foundational to research. Why don't we cite them?, https://doi.org/10.1029/2020EO151665, 2020.

Wang, H., Lin, P., Pickart, R. S., and Cross, J. N.: Summer Surface CO$_2$ Dynamics on the Bering Sea and Eastern Chukchi Sea Shelves From 1989 to 2019, Journal of Geophysical Research: Oceans, 127, e2021JC017424, https://doi.org/10.1029/2021JC017424, 2022.

Weingartner, T. J., Danielson, S. L., and Royer, T. C.: Freshwater variability and predictability in the Alaska Coastal Current, Deep Sea Research Part II: Topical Studies in Oceanography, 52, 169–191, https://doi.org/10.1016/j.dsr2.2004.09.030, 2005.

755 Whitledge, T. E., Malloy, S. C., Patton, C. J., and Wirick, C. D.: Automated nutrient analyses in seawater., Brookhaven National Laboratory, https://doi.org/10.2172/5433901, 1981.

Winkler, L. W.: Die Bestimmung des im Wasser gelösten Sauerstoffes, European Journal of Inorganic Chemistry, 21, 2843–2854, 1888.

Wright–LaGreca, M., Mackenzie, C., and Green, T. J.: Ocean Acidification Alters Developmental Timing and Gene
760 Expression of Ion Transport Proteins During Larval Development in Resilient and Susceptible Lineages of the Pacific Oyster (*Crassostrea gigas*), Marine Biotechnology, 24, 116–124, https://doi.org/10.1007/s10126-022-10090-7, 2022.

Zhang, J.–Z. and Ortner, P. B.: Effect of thawing condition on the recovery of reactive silicic acid from frozen natural water samples, Water Research, 32, 2553–2555, https://doi.org/10.1016/S0043-1354(98)00005-0, 1998.